The Astrophysical Journal, 853:84 (20pp), 2018 January 20 https://doi.org/10.3847/1538-4357/aaa54a

The Impact of Assembly Bias on the Galaxy Content of Dark Matter Halos

Idit Zehavi[1], Sergio Contreras[2,3,4], Nelson Padilla[2,5], Nicholas J. Smith[1,6], Carlton M. Baugh[3], and Peder Norberg[3,7]
[1] Department of Astronomy and Department of Physics, Case Western Reserve University, 10900 Euclid Avenue, Cleveland, OH 44106, USA; idit.zehavi@case.edu
[2] Institúto Astrofísica, Pontifica Universidad Católica de Chile, Santiago, Chile; stcontre@uc.cl
[3] Institute for Computational Cosmology, Department of Physics, Durham University, South Road, Durham, DH1 3LE, UK
[4] Centro de Estudios de Física del Cosmos de Aragón (CEFCA), Plaza San Juan 1, Planta-2, Teruel, E-44001, Spain
[5] Centro de Astro-Ingeniería, Pontificia Universidad Católica de Chile, Santiago, Chile
[6] Department of Astronomy, Indiana University, 727 E. Third Street, Bloomington, IN 47405, USA
[7] Centre for Extragalactic Astronomy, Department of Physics, Durham University, South Road, Durham, DH1 3LE, UK
Received 2017 June 23; revised 2017 December 12; accepted 2018 January 2; published 2018 January 25

Abstract

We study the dependence of the galaxy content of dark matter halos on large-scale environment and halo formation time using semi-analytic galaxy models applied to the Millennium simulation. We analyze subsamples of halos at the extremes of these distributions and measure the occupation functions for the galaxies they host. We find distinct differences among these occupation functions. The main effect with environment is that central galaxies (and in one model, also the satellites) in denser regions start populating lower-mass halos. A similar, but significantly stronger, trend exists with halo age, where early-forming halos are more likely to host central galaxies at lower halo mass. We discuss the origin of these trends and the connection to the stellar mass–halo mass relation. We find that, at fixed halo mass, older halos and to some extent also halos in dense environments tend to host more massive galaxies. Additionally, we see a reverse trend for the occupation of satellite galaxies where early-forming halos have fewer satellites, likely due to having more time for them to merge with the central galaxy. We describe these occupancy variations in terms of the changes in the occupation function parameters, which can aid in constructing realistic mock galaxy samples. Finally, we study the corresponding galaxy auto- and cross-correlation functions of the different samples and elucidate the impact of assembly bias on galaxy clustering. Our results can inform theoretical modeling of galaxy assembly bias and attempts to detect it in the real universe.

Key words: cosmology: theory – galaxies: evolution – galaxies: formation – galaxies: halos – galaxies: statistics

1. Introduction

In the standard paradigm of hierarchical structure formation, galaxies reside inside dark matter halos. The formation and evolution of these halos is dominated by gravity and can be well-predicted using high-resolution numerical simulations and in some cases analytic models. The formation of galaxies and their relation to dark matter halos is more complex and depends on the detailed physical processes leading to the various observed galaxy properties.

It has been well-established that the local halo environment of galaxies plays a fundamental role in shaping their properties. In particular, local effects are thought to be responsible for the transformation of blue, late-type, and star-forming galaxies into red, early-type, and passive galaxies (see, e.g., Oemler 1974; Dressler 1980; Lewis et al. 2002; Baldry et al. 2004; Balogh et al. 2004; Blanton & Moustakas 2009), even though there is no consensus on the relative importance of the specific processes that play a role. Different mechanisms such as mergers and interactions, ram-pressure stripping of cold gas, starvation or strangulation, and harassment all lead to changes in galaxy morphologies within the host halo environment. It is not clear, however, to what extent galaxy properties are affected by their overall "global" environment on scales larger than the individual halos. Although there is evidence that global environments affect galaxy populations—for example, red galaxies frequent high-density environments while blue galaxies are prevalent in low-density regions (e.g., Hogg et al. 2003; Blanton et al. 2005, 2006; Blanton & Moustakas 2009)—it is debatable whether the large-scale environment has an actual impact on the physical processes involved in galaxy formation and evolution.

A useful approach for studying the predictions of galaxy formation processes is with semi-analytic modeling (SAM) of galaxy formation, in which halos identified in large N-body simulations are populated with galaxies and evolved according to specified prescriptions for gas cooling, gas formation, feedback effects, and merging (e.g., Cole et al. 2000; Baugh 2006; Croton et al. 2006). These models have been successful in reproducing several measured properties such as the galaxy luminosity and stellar mass functions (see, e.g., Bower et al. 2006; Guo et al. 2011, 2013; Lacey et al. 2016). An alternative way of studying galaxy formation is using hydrodynamic simulations that follow the physical baryonic processes by a combination of fluid equations and subgrid prescriptions (see, e.g., Somerville & Davé 2015; Guo et al. 2016). Cosmological hydrodynamical simulations are starting to play a major role in the study of galaxy formation and evolution. Comparisons of such simulations with observations show broad agreement (e.g., Vogelsberger et al. 2014; Schaye et al. 2015; Artale et al. 2017).

A popular approach to empirically interpret observed galaxy clustering measurements as well as to characterize the predictions of galaxy formation theories is the Halo Occupation Distribution (HOD) framework (e.g., Peacock & Smith 2000; Seljak 2000; Scoccimarro et al. 2001; Berlind & Weinberg 2002; Cooray & Sheth 2002; Zheng et al. 2005). The HOD formalism characterizes the relationship between galaxies and dark matter halos in terms of the probability distribution, $P(N|M_{\rm h})$, that a halo of virial mass $M_{\rm h}$ contains N galaxies of a

given type, together with the spatial and velocity distribution of galaxies inside halos. The fundamental ingredient of the modeling is the halo occupation function, $\langle N(M_{\rm h})\rangle$, which represents the average number of galaxies as a function of halo mass. The typically assumed shape for the halo occupation function is motivated by predictions of hydrodynamic simulations and semi-analytic models (e.g., Zheng et al. 2005). It is often useful to consider separately the contribution from the central galaxies, namely the main galaxy at the center of the halo, and that of the additional satellite galaxies that populate the halo (Kravtsov et al. 2004; Zheng et al. 2005). The HOD approach has been demonstrated to be a powerful theoretical tool to study the galaxy–halo connection, effectively transforming measurements of galaxy clustering into a physical relation between galaxies and dark matter halos. This approach has been very successful in explaining the shape of the galaxy correlation function and its environmental dependence and overall dependence on galaxy properties (e.g., Zehavi et al. 2004, 2005, 2011; Berlind et al. 2005; Abbas & Sheth 2006; Skibba et al. 2006; Tinker et al. 2008a; Coupon et al. 2012).

A central assumption in the conventional applications of this framework is that the galaxy content in halos only depends on halo mass and is statistically independent of the halo's larger-scale environment. This assumption has its origins in the uncorrelated nature of random walks describing halo assembly in standard implementations of the excursion set formalism, which results in the halo environment being correlated with halo mass but uncorrelated with formation history at fixed mass (Bond et al. 1991; Lemson & Kauffmann 1999; White 1999). In this picture, the change in the fraction of blue and red galaxies in different large-scale environments, for example, fully arises from the change in the halo mass function in these environments (Mo & White 1996; Lemson & Kauffmann 1999). Consequently, it is not evident that global environments play a major role in directly shaping galaxy properties and in particular the HOD.

This ansatz has been challenged in the last decade by the demonstration in simulations that the clustering of halos of fixed mass varies with halo formation time, concentration, and substructure occupation (Sheth & Tormen 2004; Gao et al. 2005; Harker et al. 2006; Wechsler et al. 2006; Gao & White 2007; Jing et al. 2007; Wetzel et al. 2007; Angulo et al. 2008; Pujol & Gaztanaga 2014; Lazeyras et al. 2017). The dependence of halo clustering on properties other than the halo mass has broadly been referred to as *halo assembly bias*. The dependences on the various halo properties manifest themselves in different ways and are not trivially derived from the relations between these properties (see, e.g., Xu & Zheng 2017; Mao et al. 2018). Although predicted by ΛCDM, the exact physical origin of the assembly bias remains unclear, but different explanations have been put forth, such as correlated modes that break down the random walk assumption, statistics of peaks, and truncation of low-mass halo growth in dense environments (Keselman & Nusser 2007; Sandvik et al. 2007; Zentner 2007; Dalal et al. 2008; Desjacques 2008; Hahn et al. 2009; Lacerna & Padilla 2011; Ludlow & Porciani 2011; Zhang et al. 2014; Borzyszjowski et al. 2017).

A current topic of active debate is to what extent galaxies are affected by the assembly history of their host halos. The stochasticity in the complex baryonic physics may act to erase the record of halo assembly history. If, however, the galaxy properties closely correlate with the halo formation history, this would lead to a dependence of the galaxy content on large-scale environment and a corresponding clustering signature. This effect has commonly been referred to as *galaxy assembly bias* both colloquially and in the literature, and we adopt this distinction here. We stress, however, that what is referred to here is the manifestation of halo assembly bias in the galaxy distribution. The predictions for galaxy assembly bias have been explored with simulated galaxies (Zhu et al. 2006; Croton et al. 2007; Reed et al. 2007; Zu et al. 2008; Zentner et al. 2014; Chaves-Montero et al. 2015; Bray et al. 2016; Romano-Diaz et al. 2017). Detecting (galaxy) assembly bias is much more challenging since halo properties are not directly observed. Observational studies of assembly bias have generally produced mixed results. There have been several suggestive detections in observations (Berlind et al. 2006; Yang et al. 2006; Tinker et al. 2008b, 2017b; Wang et al. 2008, 2013b; Cooper et al. 2010; Lacerna et al. 2014a; Hearin et al. 2015; Watson et al. 2015; Miyatake et al. 2016; Saito et al. 2016; Zentner et al. 2016; Montero-Dorta et al. 2017; Tojeiro et al. 2017), while numerous other studies indicate the impact of assembly bias to be small (Abbas & Sheth 2006; Blanton & Berlind 2007; Croton & Farrar 2008; Tinker et al. 2008a, 2011; Deason et al. 2013; Lacerna et al. 2014b; Lin et al. 2016; Vakili & Hahn 2016; Zu & Mandelbaum 2016; Dvornik et al. 2017). The situation is further complicated as various systematic effects can mimic the effects of assembly bias (e.g., Campbell et al. 2015; Zu et al. 2016; Busch & White 2017; Lacerna et al. 2017; Sin et al. 2017; Tinker et al. 2017a; Zu & Mandelbaum 2017) and the evidence for assembly bias to date remains inconclusive and controversial.

Such galaxy assembly bias, if significant, would have direct implications for interpreting galaxy clustering using the HOD framework (e.g., Pujol & Gaztanaga 2014; Zentner et al. 2014), as secondary halo parameters in addition to the mass, or, more broadly, the large-scale environment in which the halo resides, would also impact the halo occupation function. For clarity, we term these variations of the halo occupation functions as *occupancy variation*. These effects are all directly related of course, as it is exactly this occupancy variation coupled with the halo clustering differences that gives rise to galaxy assembly bias.

In this paper, we aim to gain further insight into and clarify this important topic by exploring explicitly the dependence of the halo occupation functions on the large-scale environment and formation redshift in semi-analytic models. Limited work has been carried out in directly studying the environmental dependences of the HOD of galaxies, with varied results. Different works examined the dependence of the subhalo occupation on age (e.g., Jiang & van den Bosch 2017) and environment (Croft et al. 2012), which can be regarded as a proxy of the satellite occupation, if the effects of baryons are ignored. Zhu et al. (2006) explore the age dependence of the conditional luminosity function in a semi-analytic model and a hydrodynamical simulation. Berlind et al. (2003) and Mehta (2014) explore the variations of the HOD in cosmological hydrodynamical simulations, finding no detected dependence on environment. McEwen & Weinberg (2016) have recently investigated this using the age-matching mock catalogs of Hearin & Watson (2013; which by design exhibit significant assembly bias), detecting a dependence of the HOD on environment, mostly for the central galaxy occupation function.

Although the impact of assembly bias on galaxy clustering has already been demonstrated using a SAM applied to the Millennium simulation (Croton et al. 2007; Zu et al. 2008), the variation of the HOD itself with the large-scale environment or other halo properties has not been explored for it.

Here, we use the HOD formalism to directly study the impact of galaxy assembly bias as predicted by SAMs. We use the output of two independently developed SAMs, from the Munich and Durham groups, at different number densities. We measure the halo occupation functions for different large-scale environment regimes as well as for different ranges of halo formation redshift. This allows us to assess which features of the HODs vary with environment and halo age, and we present the corresponding changes in the HOD parameters. Additionally, we investigate the galaxy cross-correlation functions for these different regimes, which highlights the impact of assembly bias on clustering. Such studies will inform theoretical models incorporating assembly bias into halo models as well as attempts to determine it in observational data. Furthermore, it can facilitate the creation of mock catalogs incorporating this effect.

The outline of the paper is as follows. In Section 2, we describe the galaxy formation models used. In Section 3, we explore the dependence of the HOD on large-scale environment and halo age. We discuss the origin of the trends and the connection to the stellar mass–halo mass relation in Section 4. In Section 5, we investigate the clustering dependence on these properties, and we conclude in Section 6. Appendix A shows our halo-mass-dependent sample cuts, while Appendix B presents further measurements of the auto-correlation functions.

2. The Galaxy Formation Models

2.1. Semi-analytic Models

The SAMs used in our work are those of Guo et al. (2011, hereafter G11) and Lagos et al. (2012, hereafter L12).[8] The objective of SAMs is to model the main physical processes involved in galaxy formation and evolution in a cosmological context: (i) the collapse and merging of dark matter halos; (ii) the shock heating and radiative cooling of gas inside dark matter halos, leading to the formation of galaxy disks; (iii) quiescent star formation in galaxy disks; (iv) feedback from supernovae (SNe), from accretion of mass onto supermassive black holes and from photoionization heating of the intergalactic medium (IGM); (v) chemical enrichment of the stars and gas; (vi) dynamically unstable disks; and (vii) galaxy mergers driven by dynamical friction within dark matter halos, leading to the formation of stellar spheroids, which may also trigger bursts of star formation. The two models have different implementations of each of these processes. By comparing models from different groups, we can get a sense for which predictions are robust and which depend on the particular implementation of the galaxy formation physics (e.g., Contreras et al. 2014).

The G11 model is a version of L-GALAXIES, the SAM code of the Munich group and is an updated version of earlier implementations (De Lucia et al. 2004; Croton et al. 2006; De Lucia & Blaizot 2007). The L12 model is a development of the GALFORM Durham model (Bower et al. 2006; Font et al. 2008), which includes an improved treatment of star formation, separating the interstellar medium into molecular and atomic hydrogen components (Lagos et al. 2011). An important difference between G11 and L12 is the treatment of satellite galaxies. In L12, a galaxy is assumed to be stripped of its hot gas halo completely once it becomes a satellite and starts decaying onto the central galaxy. In G11, these processes are more gradual and depend on the destruction of the subhalo and the orbit of the satellite.

2.2. N-body Simulation and Halo Merger Trees

The SAMs used here are both implemented in the Millennium simulation (Springel et al. 2005). This simulation has a periodic volume of $(500\ h^{-1}\ \mathrm{Mpc})^3$ and contains 2160^3 particle with a mass of $8.61 \times 10^8\ M_\odot/h$ each. The simulation has 63 snapshots between $z = 127$ and $z = 0$ and was run with a ΛCDM cosmology.[9] The G11 and L12 models both use a friends-of-friends (FoF) group-finding algorithm (Davis et al. 1985) to identify halos in each snapshot of the simulation, retaining those with at least 20 particles. SUBFIND is then run on these groups to identify subhalos (Springerl et al. 2001). The merger trees differ from this point on. G11 construct dark matter halo merger trees by linking a subhalo in one output to a single descendant subhalo in the subsequent snapshot. The halo merger tree used in L-GALAXIES is therefore a subhalo merger tree. L12 employ the Dhalo merger tree construction (Jiang et al. 2014; see also Merson et al. 2013) that also uses the outputs of the FoF and SUBFIND algorithms. The Dhalo algorithm applies conditions on the amount of mass stripped from a subhalo and its distance from the center of the main halo before it is considered to be merged with the main subhalo. Subsequent output times are examined to see if the subhalo moves away from the main subhalo, to avoid merging subhalos that have merely experienced a close encounter before moving apart. GALFORM post-processes the Dhalo trees to ensure that the halo mass increases monotonically with time.

Consequently, the definition of halo mass used in the two models is not the same. The Dhalo mass used in GALFORM corresponds to an integer number of particle masses whereas a virial mass is calculated in L-GALAXIES. This leads to slight differences in the halo mass function between the models. In previous works that focused on comparing the HODs of the different models (e.g., Contreras et al. 2017), we had matched the halo mass definitions. Here, since it is not our aim to compare the HODs themselves in detail but rather examine the environmental effects on each, we prefer to leave the halo mass definitions as is, but we point out that some differences between the models are due to this. A comparison of Dhalo masses and other halo definitions is presented in Jiang et al. (2014).

3. The HOD Dependence on Environment and Halo Age

A fundamental assumption of the standard HOD approach is that the galaxy content in halos depends only on the mass of the host halo. Any dependence of the HOD on secondary parameters, like halo age or large-scale environment, is a direct reflection of galaxy assembly bias (as discussed in

[8] The G11 and L12 outputs are publicly available from the Millennium Archive in Garching http://gavo.mpa-garching.mpg.de/Millennium/ and Durham http://virgodb.dur.ac.uk/.

[9] The values of the cosmological parameters used in the Millennium simulation are $\Omega_b = 0.045$, $\Omega_M = 0.25$, $\Omega_\Lambda = 0.75$, $h = H_0/100 = 0.73$, $n_s = 1$, $\sigma_8 = 0.9$.

Section 1). In this section, we examine the impact of halo age and environment on the HOD, as predicted in the SAMs. In Section 3.1, we provide details on how the halo age and large-scale environment are defined and their relation to one another. Our main results regarding how the halo occupation functions vary with environment and halo age are presented in Section 3.2, additional cases are studied in Section 3.3, and the impact on HOD parameters is shown in Section 3.4.

3.1. Halo Formation Time and Environment

We define the formation redshift of a halo, as is commonly done, as the redshift when the main progenitor reached (for the first time) half of its present-day mass. We obtain this by following the halo merger trees of the different models and linearly interpolating between the time snapshots available. We adopt this definition to be consistent with previous studies examining the impact of halo formation time on halo assembly bias (e.g., Lemson & Kauffmann 1999; Gao et al. 2005; Zhu et al. 2006; Croton et al. 2007; Gao & White 2007). To define the large-scale environment of the halos, we use the density field obtained directly from the dark matter particle distribution with a $5h^{-1}$ Mpc Gaussian smoothing (which we denote as δ_5). This was calculated in cells of $\sim 2\ h^{-1}$ Mpc and is provided in the database. The $5\ h^{-1}$ Mpc smoothing scale is chosen as it is significantly larger than the size of the largest halos so as to reflect the large-scale environment and yet have enough different environments sampled. We also test the other smoothing radii provided in the database, 1.25, 2.5, and $10h^{-1}$ Mpc, finding the same qualitative trends we find with $5h^{-1}$ Mpc for all results shown in this paper. Alternative density and environment definitions are explored in the literature (e.g., Muldrew et al. 2012). Observationally, one naturally must resort to using the galaxy distribution to define the environment. Here, as it is available, we prefer to directly use the underlying dark matter density field, though in practice we expect our results to be insensitive to the details of the definitions.

To classify the halos by environment, we rank the halos by density in narrow (0.2 dex) bins of halo mass and select in each bin the 20% of halos that are in the densest environment and the 20% of halos in the least dense environment. This factors out the dependence of the halo mass function on environment and allows us to compare the HODs in the different environments for halos of nearly equal masses. We follow a similar procedure to select the 20% of halos with the highest and lowest formation redshifts. We illustrate how our environment and halo age cuts vary with halo mass in Appendix A. We have verified that our mass bins are sufficiently small by also using 0.1 dex bins and confirming that our results do not change. We also test splitting the sample into the 10% and the 50% extremes of the population, and find similar trends as found for the 20% subsamples.

The distribution of halos classified as residing in the 20% most and least dense environments is shown using red and blue dots, respectively, in the top panels of Figure 1, for a slice from the Millennium simulation. The remainder of the halos are shown as black dots. The dense and underdense regions appear to "carve out" disjoint regions in the cosmic web, with the densest ones being more compact than the underdense regions, as can be expected. The corresponding classification for the early- and late-forming halos, for the same slice, is shown in the bottom panels of Figure 1. It is apparent that the distribution of early- and late-forming halos is distinctly different from that of halos in dense and underdense environments. There is perhaps a tendency for the early-forming halos to preferentially occupy the dense environments, and a slight trend for late-forming halos to populate the underdense regions. However, the general distribution is very different with both early- and late-forming halos tracing well the cosmic web, in contrast to the strong environment patchy pattern. It is also clear, even by visual inspection, that the early-forming halos are more clustered than the late-forming ones. We examine the clustering of the galaxies in these halos later on in Section 5.

To further examine the correlation between formation redshift and large-scale environment, we plot in Figure 2 the joint distribution of the two properties. We do this separately for three narrow ranges of halo mass, as labelled, since the two properties by themselves also correlate with halo mass, which is apparent from the individually marginalized distributions also shown. These demonstrate the known trends that more massive halos reside in denser environments and are formed later than less massive halos. The 2D distribution appears very broad with no obvious strong trend. To quantify that we also plot the medians of one property as a function of the other: the solid lines are the median of the formation redshift for fixed density and the dashed lines the median of the environment for a given formation redshift. The fact that the solid lines are roughly horizontal and the dashed lines nearly perpendicular (or that the two sets of medians are almost perpendicular to each other) over most of the range reflects their lack of correlation with one another. This is perhaps somewhat surprising given the measurements of assembly bias (e.g., Gao et al. 2005; Gao & White 2007) showing that early-formed halos are more clustered than late-forming ones, and as such expected to reside in dense environments. Only such weak dependence is apparent, at the high-density and high-formation-redshift ends, where the two sets of lines slightly curve toward each other.

3.2. The HOD as a Function of Halo Age and Environment

It is of fundamental importance and interest to investigate how the halo occupation functions themselves vary as a function of each of these properties. For the galaxy sets, we use fixed number density samples drawn from the SAM catalogs when ranked by stellar mass. We have examined a range of different number density samples and present the results for three representative cases with number densities of $3.16 \times 10^{-2}\ h^3\ \mathrm{Mpc}^{-3}$, $10^{-2}\ h^3\ \mathrm{Mpc}^{-3}$, and $3.16 \times 10^{-3}\ h^3\ \mathrm{Mpc}^{-3}$. The corresponding minimum stellar mass thresholds for each of these are provided in Table 1. Naturally, the stellar masses increase with decreasing number density. Differences between the stellar mass values of G11 and L12 are expected, given the differences in galaxy formation prescriptions and corresponding stellar mass functions. We also provide in Table 1, as a rough guide, the median host halo mass for each such sample. In what follows, we will present the halo occupation functions for the different samples, showing separately the contributions from central galaxies and satellites. The general form expected for stellar mass threshold samples is a smoothed step function for the occupation function of the centrals and roughly a power-law for the occupation function of the satellites (see also Section 3.4).

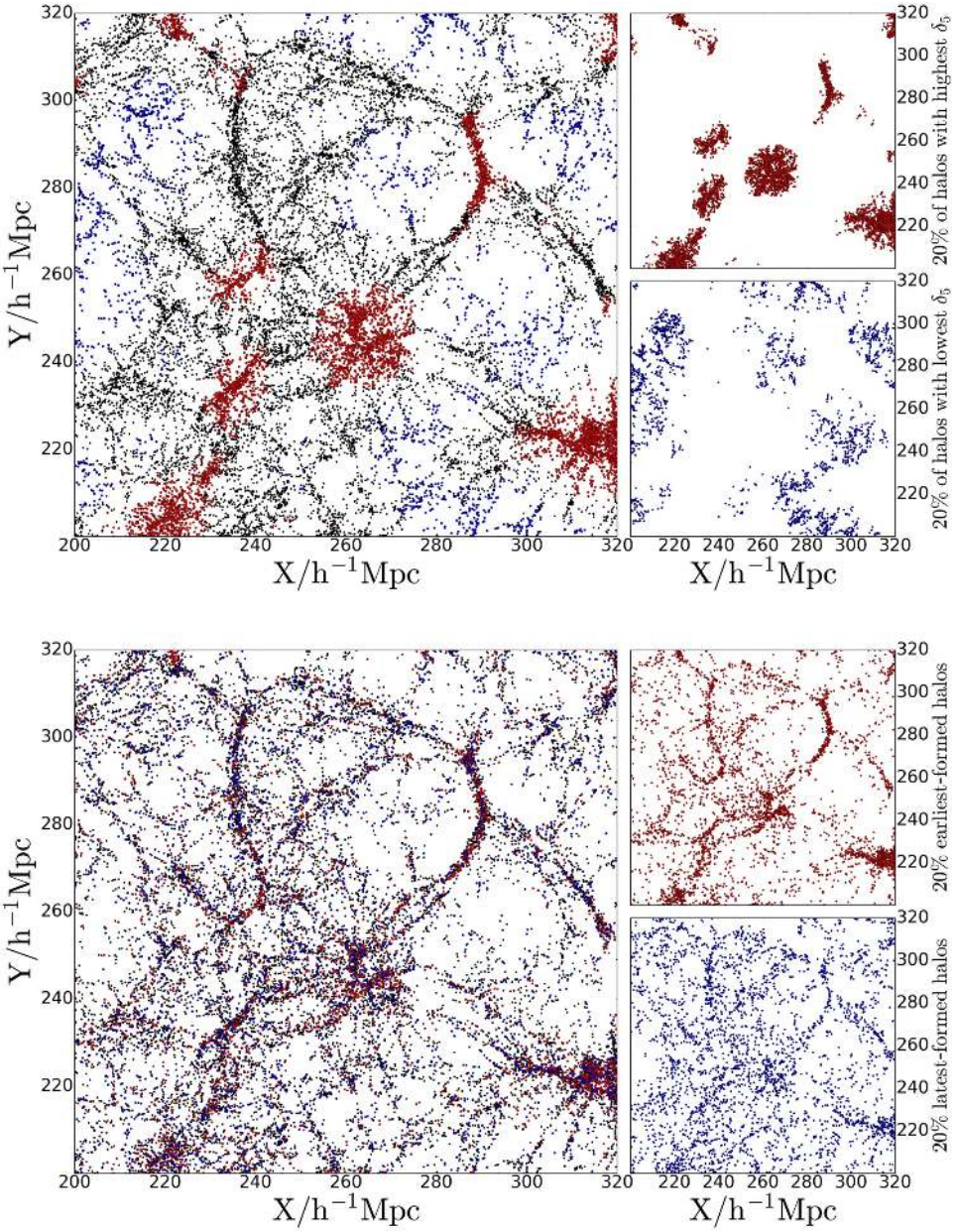

Figure 1. Top panels: a 120 h^{-1} Mpc × 120 h^{-1} Mpc × 20 h^{-1} Mpc slice of the Millennium simulation showing the distribution of the halos in it. Red (blue) dots represent the 20% of halos that live in the densest (least dense) environments, and the remainder are represented by the black dots. The density selection is made in 0.2 dex bins of fixed halo mass (see the text). The bigger plot on the left includes all halos, while the smaller ones on the right-hand side show separately only the 20% of halos that live in the densest and least dense environments. Bottom panels: same as in the top panels, for an identical slice from the Millennium simulation, but now color-coding halos by formation time instead of environment. Red (blue) dots represent the 20% earliest (latest) formed halos.

Figure 3 shows how the halo occupation functions vary with environment and halo age for the galaxy sample from the G11 SAM model with a number density of 10^{-2} h^3 Mpc^{-3}. The left panel shows the HODs for the full galaxy sample (black) as well as for the subsets of galaxies that reside in the 20% of halos in the densest environments (red) and the 20% of halos in the least dense environments (blue). We remind the reader that the division into 20% most/least dense regions is done for each bin of halo mass, so that the different samples equally probe the full halo mass range. Also, we note that, by construction, these samples have equal numbers of halos but not equal numbers of galaxies.

We find distinct differences in the HODs for both the central and satellite occupation functions. For the central occupation, the differences are noticeable at the "knee" of the occupation function and below. We find that in the densest environments, central galaxies are more likely to reside also in lower-mass halos, and the trend reverses in underdense regions. Stated in a slightly different way, in the regime where the halo occupation rises from 0 to 1, halos are more likely to host central galaxies if they reside in dense environments. This may be related to the preferential early formation of halos in dense regions, although as we saw above the correlation is rather loose. We discuss below further insight into the resulting trends for central galaxies (see Section 4).

The satellite occupation function in the G11 model also exhibits a dependence on large-scale environment. The satellite occupation function in dense environments exhibits a slight

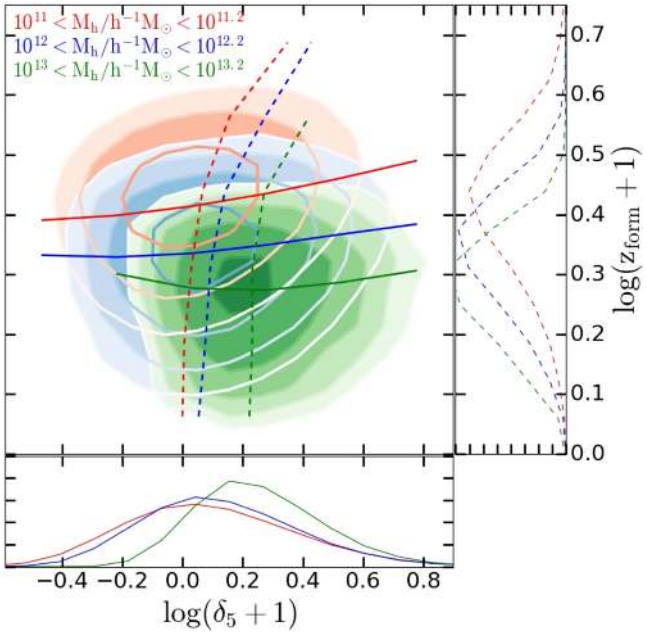

Figure 2. Joint distribution of large-scale environment (δ_5) and formation redshift (z_{form}) for present-day halos in the Millennium simulation, for three narrow ranges of halo mass. The red, blue, and green contours represent halos with low, intermediate, and high masses, respectively, as labelled in the top part of the figure. The different contour levels correspond to 1σ, 2σ, and 3σ of the distribution. The marginalized distributions of each property are shown separately as well, for each halo mass bin. The (roughly horizontal) solid lines represent the median values of the formation redshift as a function of environment. The (roughly perpendicular) dashed lines are the median values of environment at each formation redshift.

Table 1
Stellar Mass Thresholds (Top) and Median Halo Masses (Bottom), All in Units of $h^{-1}\,M_\odot$, for the Three Main Number Density Samples (in units of h^3 Mpc^{-3}) Presented in This Work, for the G11 and L12 Models

		3.16×10^{-2}	1×10^{-2}	3.16×10^{-3}
G11	$M_*^{\min}$	1.85×10^{9}	1.42×10^{10}	3.88×10^{10}
L12	$M_*^{\min}$	9.39×10^{8}	6.50×10^{9}	2.92×10^{10}
G11	$\tilde{M}_h$	2.70×10^{11}	8.74×10^{11}	2.69×10^{12}
L12	$\tilde{M}_h$	3.66×10^{11}	1.23×10^{12}	3.89×10^{12}

shift toward larger numbers, so that halos in dense environments are more likely to have more satellites on average. This behavior is perhaps naturally expected, due to the increased interactions and halo mergers in dense environments.

The right panel of Figure 3 shows how the occupation function varies with halo age for the same G11 galaxy sample with number density $10^{-2}\,h^3$ Mpc^{-3}. In the case of halo age, there are much larger effects on the occupation functions than we saw with environment. For the central occupation, we find a clear trend of early-forming (old) halos being more likely to host galaxies at lower masses than late-forming (young) halos. This likely arises from the fact that the early-formed halos have more time for stars to assemble and for the galaxy to form. The sense of the trend is the same as that for the environmental dependence but is a much stronger one, with the "shoulder" of the occupation function extending significantly toward lower masses with older age.

We find a strong reverse effect for the satellite occupation at the low-mass end: early-forming halos have significantly fewer satellites than late-forming halos. This trend is pronounced at low occupation numbers of $\langle N(M_h)\rangle < 10$ and becomes negligible at higher occupation numbers. This is probably due to the fact that in the early-forming halos, there is simply more time for the satellites to merge with the central galaxy, which will be a more dominant process at the low halo mass/low occupation regime. This trend is similar to the predicted dependence of subhalo occupation on halo formation time (van den Bosch et al. 2005; Zentner et al. 2005; Giocoli et al. 2010; Jiang & van den Bosch 2017), indicating that baryonic physics does not play an important role in the variation of the satellite occupancy.

These differences in the halo occupation functions, for both age and environment, are significant. We estimate the uncertainties on the HOD calculations using jackknife resampling, dividing the full simulation volume into 10 slices. Incidentally, when separating the different subregions, if the center of a given halo is in a certain subvolume, we include with it all galaxies in that halo, regardless of where the physical boundary between the subvolumes lie. The resulting errors are shown as shaded regions in the figure and are in fact negligible over most of the range and only become significant at the high-mass range where the number of halos is small.

The HOD dependences on age and environment are different in magnitude (for centrals) and sense (for satellites). The strength of the trends with age versus environment perhaps indicates that formation time is the more fundamental property related to assembly bias. Varying the Gaussian-smoothing length used to define the environment impacts slightly the size of the deviations, with the differences becoming a bit more pronounced for small smoothing lengths, as expected. However, we choose to stick with our $5h^{-1}$ Mpc Gaussian smoothing so as to robustly infer the large-scale environment.

We describe and model these differences in terms of the HOD parameters in Section 3.4. The dependence on environment we find for the central occupation is very similar to that measured by McEwen & Weinberg (2016). However, they do not find any noticeable difference for the satellite occupation. Our results differ from those of Mehta (2014), who find no significant dependence of the HOD on environment. The level of occupancy variation that is present appears to depend on the specifics of the galaxy formation model utilized.

3.3. The HOD for Different Models and Samples

To further investigate the dependence on the galaxy formation model, we repeat the analysis in Section 3.2 using the independently derived L12 Durham model. Figure 4 shows the HOD dependence on environment and halo age for a galaxy sample with number density of $10^{-2}\,h^3$ Mpc^{-3} from the L12 SAM. The environmental dependence for L12 shows a similar trend for the central occupation, while the trend for satellite occupation disappears. The difference in the satellite occupations between L12 and G11 could arise due to the different treatment of satellites in the two models (Section 2.1). As the satellite destruction processes are more immediate in L12, perhaps there is less time for the environmental effects to impact the occupation in that case.

The HOD dependence on halo formation time for L12 and G11 is very similar, with L12 showing the strong trends for both the central and satellite occupations as well. The tendency of centrals to shift toward occupying lower-mass halos is slightly stronger for L12. We note the distinct change of shape of the central occupation, giving rise to a non-monotonic

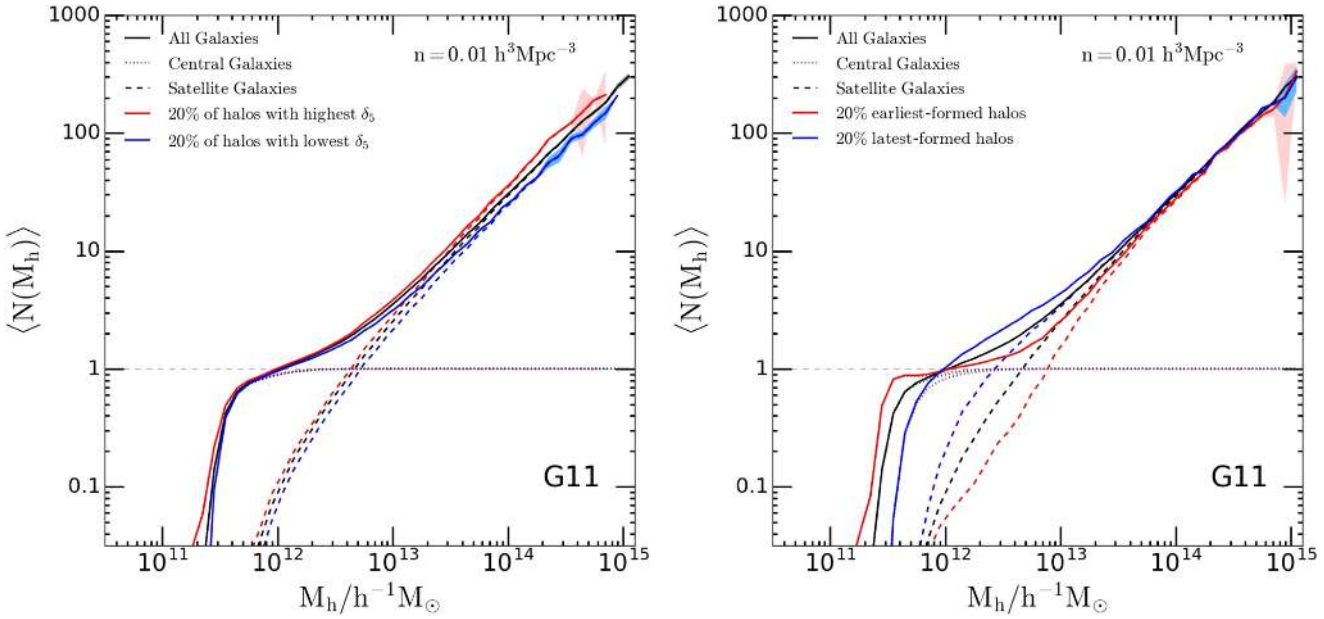

Figure 3. Left panel: the halo occupation functions for a stellar-mass-ranked galaxy sample corresponding to a number density of 10^{-2} h^3 Mpc^{-3} for the G11 model. The solid black line shows the HOD of all galaxies in the sample. The solid red line shows the HOD for the galaxies in the 20% of halos in the densest environments, while the solid blue line presents the HOD for the galaxies in the 20% of halos in the least dense environments. The red and blue shaded regions (apparent only at the high-mass end) represent the jackknife errors calculated using 10 subsamples. In all cases, the dotted lines show separately the central galaxy occupation contribution and the dashed lines represent the satellite occupation. Right panel: same as in the left panel, but for halo samples selected by their formation time instead of their environment. The occupation function for galaxies in the 20% earliest-formed halos is shown in red, and that for the 20% latest-formed halos is shown in blue.

occupation for the galaxies in early-forming halos. This is likely to be related to the form of active galactic nuclei (AGN) feedback in the Durham models, as discussed in McCullagh et al. (2017).

We also examine the dependence of the different trends with the stellar mass of the galaxies by varying the number density of the samples. As the samples are ranked by stellar mass, larger number densities include smaller stellar masses, while small number densities are limited to more massive galaxies. Figures 5 and 6 present our results for environment and age, respectively, for two additional number densities (one smaller and one larger). In both cases, the HODs change globally as expected, shifting overall toward lower halo masses with increasing number density (decreasing stellar mass).

The specific signatures of the environmental dependence of the HOD change as well with number density. For G11 (top panels of Figure 5), the differences in the central occupations increase with number density. This is in accordance with the findings of Croton et al. (2007) that galaxy assembly bias is stronger for fainter (less massive) galaxies. For the lowest number density shown, corresponding to galaxies with stellar masses larger than $3.88 \times 10^{10}\,h^{-1}\,M_\odot$ (Table 1), the differences between the central occupations are barely noticeable. In contrast, the G11 satellite occupation differences decrease slightly with number density. These opposing changes with number density suggest that the environment dependence of the central and satellite occupations have different origins. We find a similar change with number density of the central occupation environment dependence for L12 (bottom panels of Figure 5), while the satellite occupancy variation remains effectively undetected.

The halo age signatures for the different number densities (Figures 3, 4, and 6) are quite robust and do not exhibit any clear dependence on the number density for either model, again indicating that these may be of a different physical nature from the environment occupancy variations. The non-monotonic occupation behavior for the early-forming halos (McCullagh et al. 2017) is also apparent in the smallest number density case for the G11 model.

3.4. Extending the HOD Parametrization

It is customary to parametrize the shape of the HOD using a five-parameter model that captures the main features of the halo occupation function, as predicted by SAMs and hydrodynamic simulations (Zheng et al. 2005). This model is commonly used when interpreting galaxy clustering measurements to infer the galaxy–halo connection (e.g., Zheng et al. 2007; Zehavi et al. 2011). Here, we characterize the HOD dependences on age and environment in terms of the five parameters as a first step toward incorporating these variations into the HOD model.

The halo occupation function is usually modeled separately for central galaxies and satellites. The occupation function for centrals is a softened step-like function with the following form:

$$\langle N_{\rm cen}(M_{\rm h})\rangle = \frac{1}{2}\left[1 + {\rm erf}\left(\frac{\log M_{\rm h} - \log M_{\rm min}}{\sigma_{\log M}}\right)\right], \qquad (1)$$

where erf(x) is the error function, ${\rm erf}(x) = \frac{2}{\sqrt{\pi}}\int_0^x e^{-t^2}dt$. $M_{\rm min}$ characterizes the minimum halo mass for hosting a central galaxy above the specified threshold. In the form adopted here, it is the halo mass for which half of the halos are occupied. $\sigma_{\log M}$ indicates the width of the transition from zero to one galaxy per halo and reflects the scatter between stellar mass and halo mass.

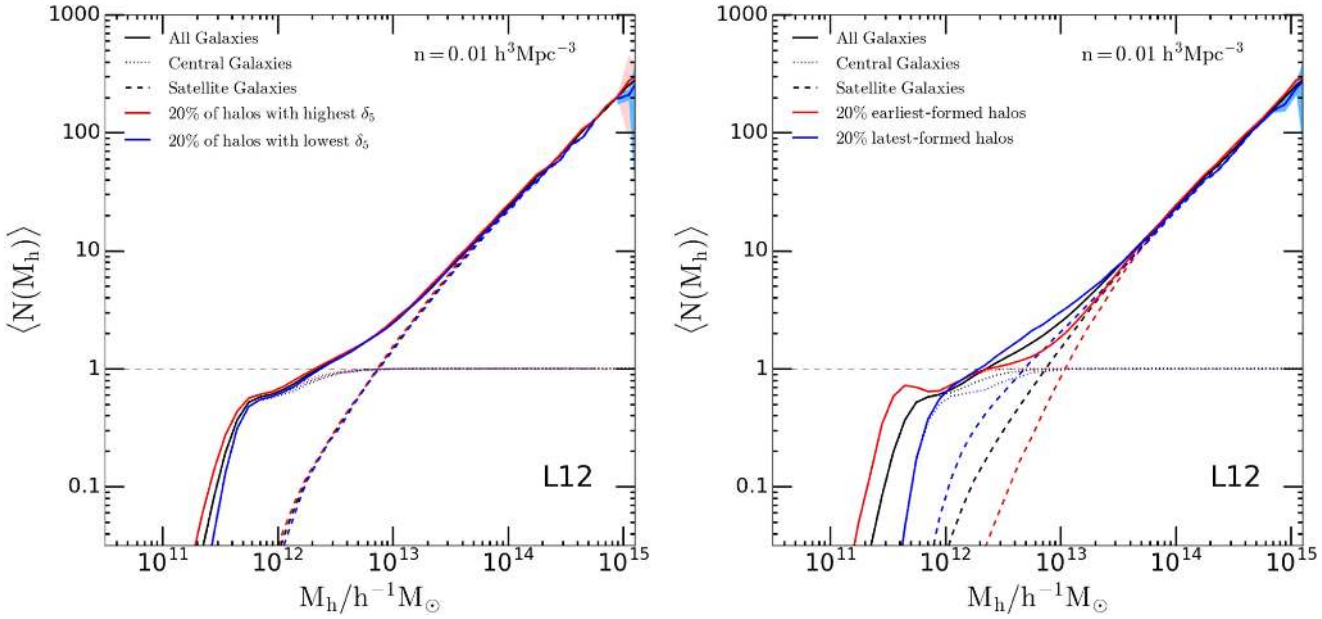

Figure 4. Same as Figure 3 but for the L12 model.

For satellite galaxies, the occupation function is modeled as

$$\langle N_{\rm sat}(M_{\rm h})\rangle = \left(\frac{M_{\rm h} - M_{\rm cut}}{M_1^*}\right)^{\alpha}, \quad (2)$$

for $M_{\rm h} > M_{\rm cut}$, representing a power-law occupation function with a smooth cutoff at the low-mass end. Here, α is the slope of the power law, with typical values close to one, $M_{\rm cut}$ is the satellite cutoff mass scale (i.e., the minimum mass of halos hosting satellites), and M_1^* is the normalization. Often, instead of the latter, a related parameter, M_1, is used, which is the mass of halos that host one satellite galaxy on average ($M_1 = M_1^* + M_{\rm cut}$). The total occupation function is then specified by these five parameters and given by the sum of the two terms:

$$\langle N_{\rm gal}(M_{\rm h})\rangle = \langle N_{\rm cen}(M_{\rm h})\rangle + \langle N_{\rm sat}(M_{\rm h})\rangle. \quad (3)$$

Note that we are using here the form as originally proposed by Zheng et al. (2005), which allows the central and satellite occupation functions to be fitted independently.

One relation that is often examined in this context is the ratio between the two characteristic halo masses, $M_1/M_{\rm min}$ (e.g., Zheng et al. 2005; Seo et al. 2008; Zehavi et al. 2011; Guo et al. 2014; Skibba et al. 2015; Contreras et al. 2017). This ratio, which measures how much more massive a halo has to be in order to host an additional galaxy beyond the central one, broadly reflects the balance between the accretion and destruction of satellites and impacts the shape of the correlation function (Zentner et al. 2005; Seo et al. 2008; Watson et al. 2011).

Figure 7 shows how these five parameters vary with environment. The left-hand side presents the HOD of the G11 SAM for $n = 3.16 \times 10^{-2}\ h^3\ \mathrm{Mpc}^{-3}$ for the full sample, and the 10% of halos in the densest regions and the 10% of halos in the least dense regions. The dots represent the directly measured HODs, and the lines are the best-fit five-parameter models to them. The right-hand side examines how each of the parameters varies with environment in 10% bins of the halo environment. The fits are done assuming equal weight to all measurements and using only those with $\langle N(M_{\rm h})\rangle > 0.1$. The error bars on the parameters are obtained by requiring $\chi^2/\mathrm{dof} = 1$, as in Contreras et al. (2017).

For this G11 sample, we see that the changes to the parameters when varying the environment are subtle, but all are affected. The changes in the central occupation with density are in fact quite small, with $M_{\rm min}$ decreasing and $\sigma_{\log M}$ increasing slightly with density. The variations in the best-fitting parameters are influenced by the limited flexibility in the assumed shape of the HOD. The changes in the satellite occupation with increasing density act to gradually decrease $M_{\rm cut}$ and M_1 and increase the slope α, over at least part of the density range. We note that we find more intricate changes to the HOD parameters than those modeled in McEwen & Weinberg (2016), since that work saw differences only in the occupation function for central galaxies and not the one for satellites. The resulting variation in the $M_1/M_{\rm min}$ ratio (bottom-right panel) is a noticeable decrease with increasing density over most of the range, but then a turnover and a slight increase for halos in the densest regions.

Figure 8 examines the change in the parameters, but now with halo formation time. The change in parameters in this case is more distinct and significant, since the dependence of the HOD on halo age is stronger than that on the environment. $M_{\rm min}$ monotonically decreases with increasing formation redshift (earlier formation). $\sigma_{\log M}$ varies with halo age but does not show a clear trend. The satellite occupation changes in the opposite sense, with all three parameters $M_{\rm cut}$, M_1, and α increasing significantly with larger formation redshift. (The change in the slope α again may be somewhat affected by the limitations of the assumed HOD shape.)

The combined effect on the $M_1/M_{\rm min}$ ratio is a dramatic increase with formation redshift, of about a factor six over the full range! This change is much stronger than the variation of this ratio with either number density or redshift, about twice as large as the variation with number density and close to four

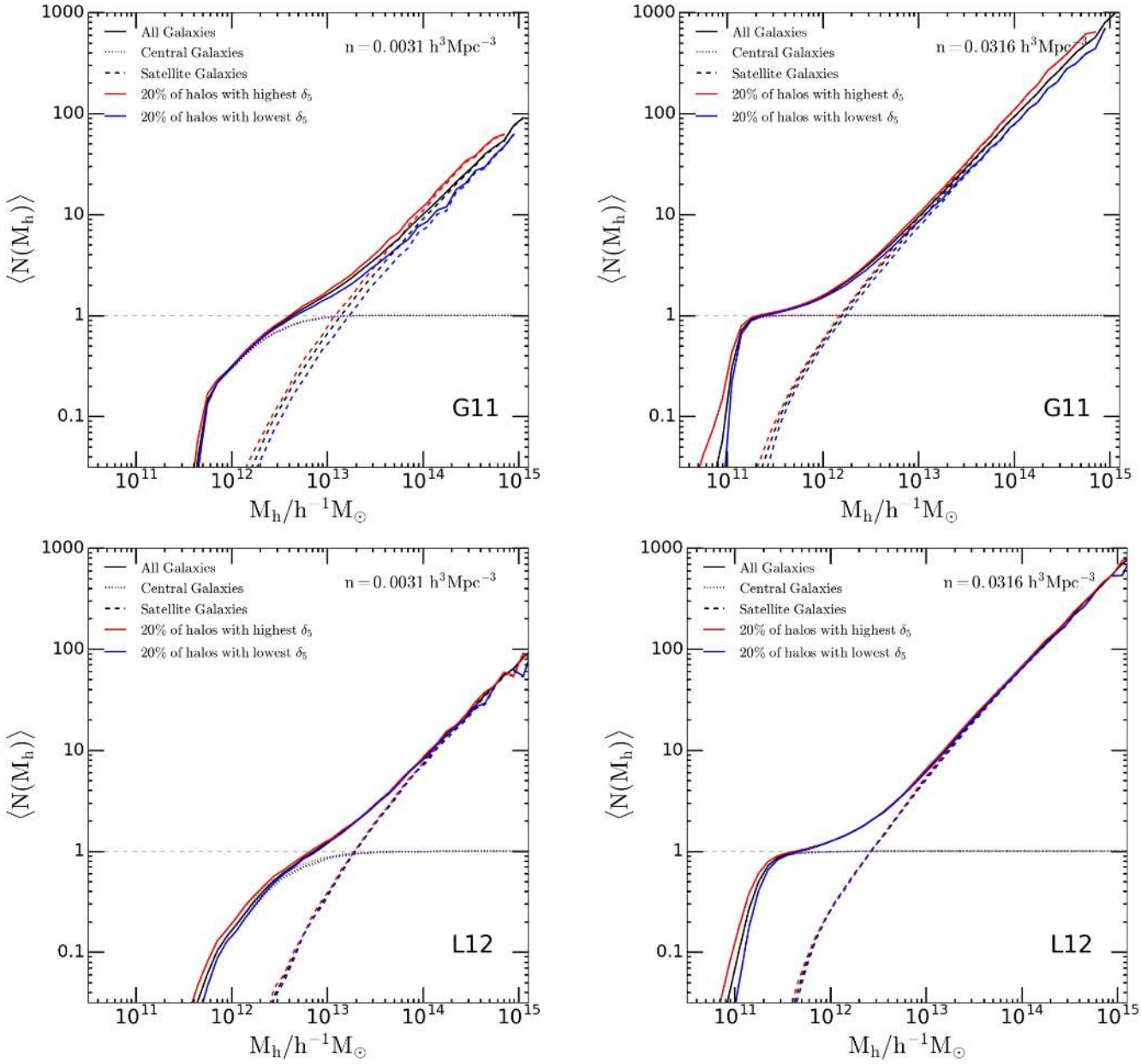

Figure 5. Dependence of the halo occupation functions on large-scale environment for number densities different from that shown in Figures 3 and 4, $3.16 \times 10^{-3}\ h^3$ Mpc^{-3} on the left-hand side and $3.16 \times 10^{-2}\ h^3$ Mpc^{-3} on the right-hand side. The top panels are for the G11 model and the bottom ones are for L12.

times larger than the evolution in the ratio from redshift 3 to 0, as explored by Contreras et al. (2017). This significant change, however, is easily understood from the predicted occupancy variation (e.g., right part of Figure 3). For earlier-forming halos, M_1 shifts toward larger halo masses while $M_{\rm min}$ shifts toward smaller halo masses, resulting in a substantial increase in their ratio. Still, it is noteworthy that the $M_1/M_{\rm min}$ ratio is such a sensitive indicator of halo age.

These results can inform theoretical modeling efforts extending the standard HOD framework. We can envision modeling the change of each parameter with halo age as a power-law function with an additional assembly bias parameter (similar to our modeling of the evolution of the HOD in Contreras et al. 2017). Such a model may aid in obtaining constraints on assembly bias from observational data as well as provide a method of incorporating environment and age dependence of the HOD into galaxy mock catalogs.

4. The Stellar Mass–Halo Mass Relation

To gain a better understanding of the origin of the trends seen in the central galaxy occupation function with age and environment, we examine the stellar mass—halo mass (SMHM) relation. As we show, it is the dependence of the scatter in this relation on the secondary parameters that gives rise to the occupancy variation and to galaxy assembly bias.

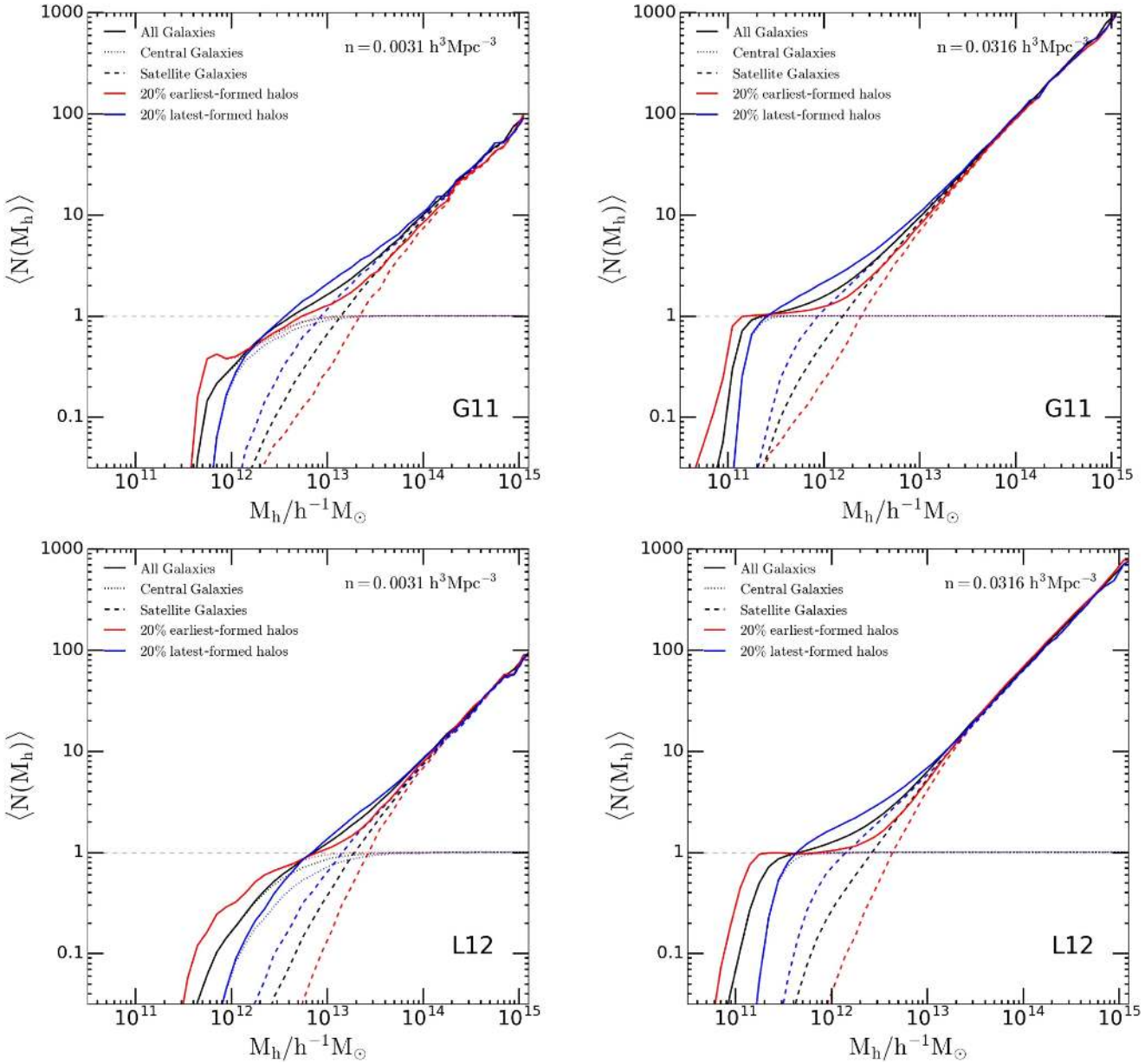

Figure 6. Same as Figure 5, but for galaxy samples selected using halo formation time instead of environment.

Figure 9 shows the stellar mass of central galaxies as a function of halo mass for galaxies in the G11 SAM. We plot 1% of all central galaxies, for clarity. The stellar mass increases with halo mass, with the median of the relation (black line) exhibiting a relatively steep slope up to $M_{\rm h} \sim 10^{12}\,h^{-1}\,M_{\odot}$ and a shallower increase for more massive halos, when the AGN feedback becomes important. This was studied in detail in Mitchell et al. (2016) for GALFORM (see also Contreras et al. 2015). There is a significant scatter in the relation, which decreases at the high-mass end. This scatter is expected to be due to stochasticity in both galaxy and halo assembly histories and the various physical processes. Thus, we may expect the scatter to be related to the properties of the host halos. We examine this visually by color-coding each galaxy by its large-scale environment (top panel) and by the formation redshift of its host halo (bottom panel).

As is apparent from Figure 9, the spread around the median SMHM relation is not random but depends on the secondary property. For halos less massive than about $10^{12}\,h^{-1}\,M_{\odot}$, there is an apparent dependence on the large-scale environment (top panel), where for a fixed halo mass, more massive central galaxies tend to reside in denser environments. This trend appears to have a fairly sharp transition between relatively low and high densities, even though there is a large scatter of different environments at each location on the SMHM relation (as is evident by the mix of colors). The trend does not persist toward larger masses, where there is no variation of environment for a fixed halo mass (or else it is impossible to see one due to the large scatter of the different densities). We find that the central galaxies in the densest environments (in absolute terms, not per halo mass bin, i.e., the red/maroon colored ones in the top panel) populate two distinct regions in this diagram:

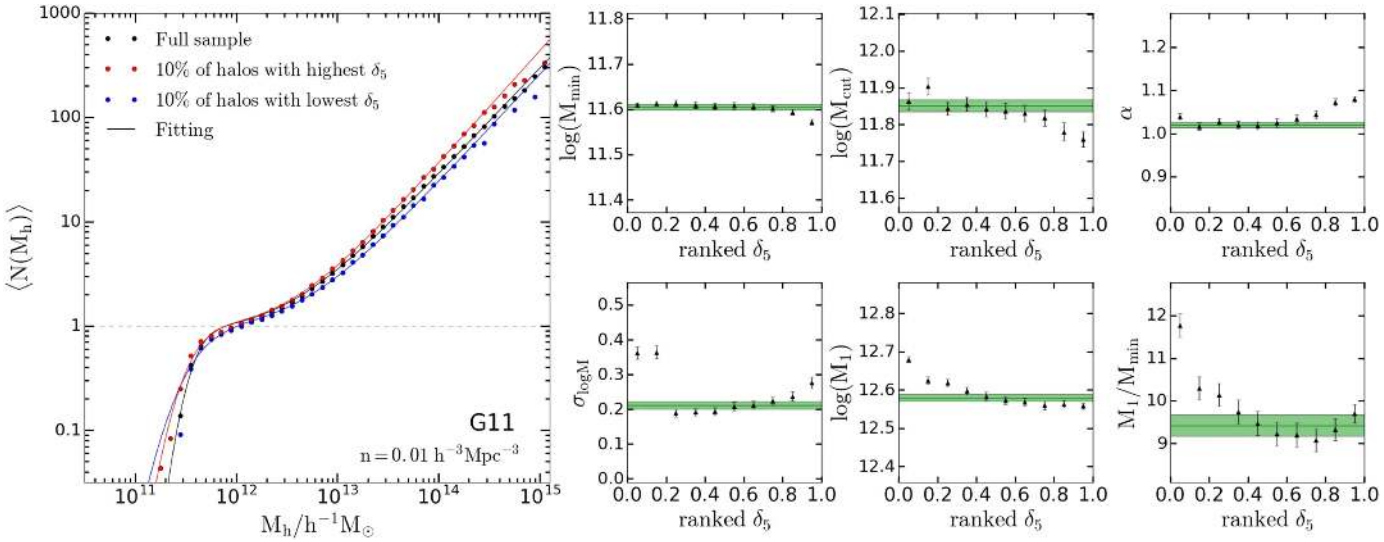

Figure 7. Left: the HOD of the G11 SAM for a number density of $3.16 \times 10^{-2}\,h^3$ Mpc^{-3}. Dots represent the HOD calculated in the simulation: the black ones show the HOD for all galaxies, the red ones the HOD for the 10% of halos in the densest environments, and the blue ones show the HOD for the 10% of halos in the least dense environments. The solid lines, in corresponding colors, show the five-parameter best-fit models for these. Right: the values of the best-fitting parameters of the HODs as a function of the environment percentile for $M_{\rm min}$ (top left), $\sigma_{\log M}$ (bottom left), $M_{\rm cut}$ (top middle), M_1 (bottom middle), α (top right), and $M_1/M_{\rm min}$ (bottom right). Each dot in these plots represents a different subsample selected by its large-scale environment, each with 10% of the full halo population, with the environment density increasing from left to right. The leftmost dots and rightmost dots in these panels represent the parameter values of the models plotted in blue and red, respectively, in the left-hand side HOD panel. The error bars reflect the 1σ uncertainty on the parameters. The green horizontal lines with shaded regions in the parameter panels are the values fitted for the full sample and their uncertainty.

they predominantly populate the most massive halos, albeit at smaller numbers according to the halo mass function, and they also comprise the most massive centrals in low-mass halos. The former simply stems from the fact that the most massive halos tend to reside in dense environments, while the latter is related to the occupancy variation we discuss here.

The bottom panel of Figure 9 shows the same SMHM relation, but now color-coded by the formation redshift (age) of the halos. The trend with halo age for a fixed halo mass is particularly striking, with more massive central galaxies generally residing in halos that formed early. This dependence on halo age is gradual but very distinct, due to the small scatter of halo ages at each location in the SMHM diagram for halos below $\sim 10^{12}\,h^{-1}\,M_\odot$. The trend persists for all halo masses, but with a significantly larger scatter of halo ages at the high-mass end, as the formation redshifts also progressively become more recent, as expected. A similar trend with halo formation time has already been measured in SAMs (Wang et al. 2013a; Tojeiro et al. 2017) and also for galaxies in the EAGLE hydrodynamical simulation (Matthee et al. 2017). It likely arises because central galaxies in early-formed halos have more time for accretion and star formation and thus end up being more massive. Once again, it appears that halo age is the more fundamental characteristic here that affects galaxy properties.

The dependence on environment is more complex and harder to interpret. Jung et al. (2014) investigate the stellar mass dependence on environment for fixed halo mass using a different SAM. They find only small differences between halos in the densest and least dense environments for low halo masses, and these differences diminish with increasing halo mass (cf., Tonnesen & Cen 2015). This suggests that the level of secondary correlations present (and by association, galaxy assembly bias) depends on the details of the galaxy formation model adopted. We note also the counterintuitive fact that, at least according to the study of Matthee et al. (2017), while some fraction of the scatter in the SMHM relation is accounted for by formation time, the large-scale environment seems to make a negligible contribution.

The fundamental importance of these dependences of stellar mass on secondary properties at fixed halo mass is that they provide a direct explanation for the central galaxy occupancy variation with environment and halo age (as shown in, e.g., Figure 3). For a fixed halo mass, early-formed halos or halos in denser environments host more massive galaxies. Consequently, any fixed stellar mass cut (e.g., the $1.42 \times 10^{10}\,h^{-1}\,M_\odot$ threshold used to define the $n = 10^{-2}\,h^3\,{\rm Mpc}^{-3}$ sample analyzed in Figure 3) would include these first. Thus, the central galaxies in early-forming halos or dense environments populate relatively lower-mass halos, extending the central occupation function in that direction. And, conversely, late-forming halos or halos in underdense environments generally host lower-mass galaxies. Therefore, only centrals hosted by more massive halos will make it into the sample, and the central occupation function in that case will be shifted toward more massive halos.

The level of scatter in halo age or environment at each location directly determines the strength of the occupancy variation. The tight correlation between stellar mass and halo age (for a fixed halo mass) results in a large variation of the HOD, while the large scatter involved with environment results in only a moderate change of the HOD in that case. Furthermore, as noted already, the SMHM trend with environment holds only at the low-mass end, while the general trend with halo age persists for all halo masses. This explains the change in occupancy variation with number density, demonstrated in Figures 5 and 6. For age, the occupancy

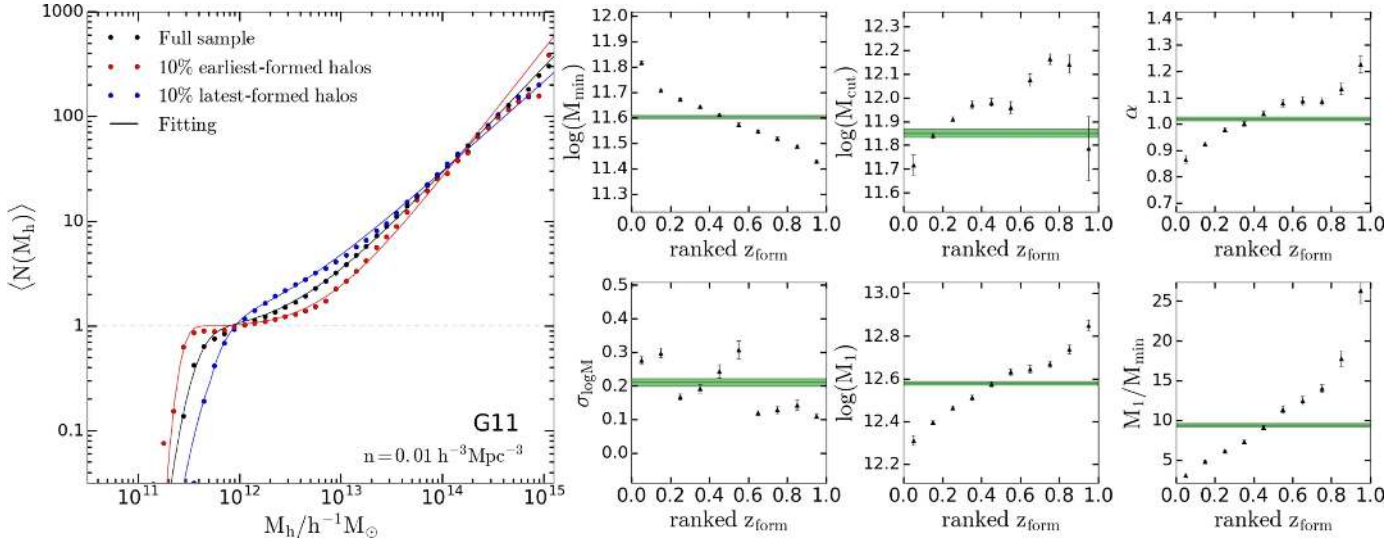

Figure 8. Same as Figure 7, but for subsamples selected by halo formation time instead of large-scale environment. In the panels for the individual parameters, the halo formation redshift (age) increases going from left to right. Please note that for the parameter values on the right, the *y*-axis ranges are different from those of Figure 7.

variation remains at comparable levels for all number densities, similar to the trend in the SMHM relation. For environment, the level of occupation variation decreases for smaller number densities (larger stellar mass thresholds) as these correspond to larger halo masses where the trend with environment diminishes.

In any case, we are seeing that the correlated nature of the scatter in the SMHM relation is intimately related to the trends in the occupation functions. It is exactly this coupling between halo properties (such as large-scale environment and formation time) and galaxy properties (such as stellar mass or luminosity) that causes the dependence of the HOD on halo assembly. A more extensive study of the connection between the SMHM relation and the occupancy variation and galaxy assembly bias will be presented elsewhere (I. Zehavi et al. 2018, in preparation).

5. The Impact on Galaxy Clustering

To see the impact of the occupancy variation with halo age and environment (Section 3) on galaxy clustering, we measure and examine the correlation functions of galaxies in these samples. The variations in the HODs couple with the different clustering properties of the halos to produce a signature of galaxy assembly bias in the galaxy distribution.

5.1. The Shuffling Mechanism

To measure the effects of assembly bias on the galaxy correlation function, we need to create a control sample of galaxies where we explicitly remove the galaxy assembly bias, and then compare to the clustering of the original sample. In order to do that, we shuffle the full galaxy population among halos of similar masses, following the procedure of Croton et al. (2007). Specifically, we select halos in 0.2 dex bins of halo mass and randomly reassign the central galaxies hosted by these halos among all halos in that mass bin. The satellite galaxies are moved together with their original central galaxy, preserving their distribution around it. For any stellar mass threshold sample, this is equivalent to randomly reassigning the galaxy content of the halos among all halos of similar mass, including the ones that were initially unoccupied. The shuffling thus eliminates a dependence of the galaxy population on any inherent properties of their host halos other than mass. Effectively, what the shuffling does is remove the occupancy variation, namely the dependence of the HOD on halo properties other than mass. For these shuffled samples, the HOD of the full galaxy sample remains the same, but the differences between the HODs of different halo populations, e.g., split by age or environment, are now eliminated and all share the same HOD as the full sample.

We have verified that the results we present below are insensitive to our specific choice of bin size in halo mass. We also note that alternative shuffling algorithms have been proposed in the literature, where the satellites are also shuffled among different halos of the same mass independent of the central galaxies (e.g., Zu et al. 2008; Zentner et al. 2014). This additional satellite shuffling is important only when one is specifically concerned with features that correlate the properties of centrals and satellites or the satellites with themselves, such as galactic conformity or satellite alignment. For our purposes, the combined central+satellite galaxies shuffling completely suffices to erase the signature of occupancy variation. We clarify that our shuffling does impact the small scales (one-halo term) of the correlation function of our subsamples, as we show below (in contrast to the statement made in some works that this shuffling preserves the one-halo term, which only holds when considering the full galaxy sample).

5.2. The Correlation Functions

Figure 10 presents our main results regarding the dependence of clustering on large-scale environment and halo age and the impact of assembly bias. It is based on the calculated auto-correlation function of the full galaxy sample and the cross-correlation functions of the different galaxy subsamples (in the 20% subsets of halos) with the full galaxy sample. Appendix B

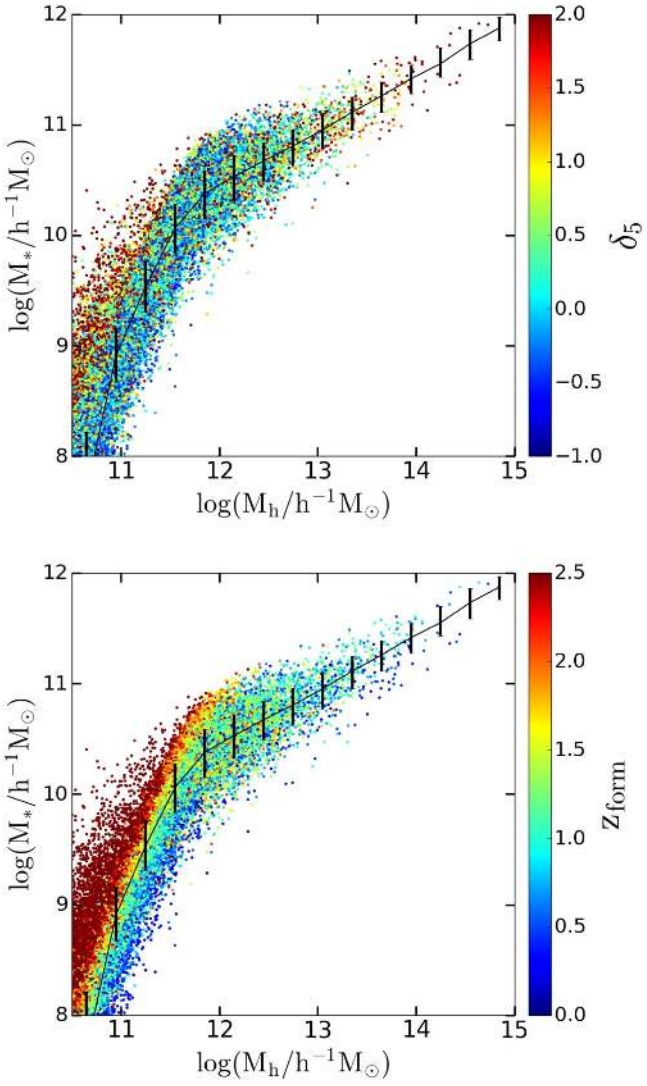

Figure 9. Top: the stellar mass of central galaxies as a function of host halo mass for the G11 SAM and its dependence on environment. Each dot represents a central galaxy, plotted for a representative (randomly chosen) 1% of the galaxies. Galaxies are color-coded by their $5\,h^{-1}$ Mpc Gaussian-smoothed density, δ_5, according to the color scale shown on the right. The black solid line represents the median of the distribution with the error bars designating the 20%–80% range of the distribution. Bottom: same as for the top panel, but now color-coded by the formation redshift, calculated as the time when the halo reaches half of its final mass. For a fixed halo mass, more massive central galaxies tend to live in halos that formed early or reside in denser environments (with the latter being a weaker trend than the former).

presents the corresponding figure for the auto-correlation functions of the full galaxy sample and of the different galaxy subsamples on their own, for the halo-age case. This appendix serves to motivate our choice to focus on the cross-correlation results in the main text. Throughout, the auto-correlation functions are estimated by calculating DD/RR − 1, where DD represents the number of data–data pairs and RR represents the number of random–random expected pairs, estimated analytically. This simple estimate is fine for our purposes, since there are no issues here with edge effects or uncertainties in the galaxy density, which typically require more evolved estimates in observational data. The cross-correlation functions are obtained in an analogous fashion using $D_1D_2/R_1R_2 - 1$.

Figure 10 shows the correlation functions measured for the galaxy subsamples analyzed in Figure 3, for the $n = 10^{-2}\,h^3\,\mathrm{Mpc}^{-3}$ sample from the G11 SAM. We present the auto-correlation function of the full galaxy sample (solid black lines) and the cross-correlation function between the full sample and the different subsets of galaxies (red and blue solid lines, as labelled), showing the environmental dependence on the left and formation time on the right. The dashed lines in all cases show the results when shuffling the galaxy samples, effectively removing the occupancy variation, as described in Section 5.1. The top subpanels are the correlation functions themselves, and the middle and bottom subpanels show the ratios derived from these correlation functions to highlight different features as described in the figure caption and discussed below.

The shaded regions represent the uncertainties on these measurements estimated from jackknife resampling, when dividing the full simulation volume into 10 slices along one axis (identical subvolumes to those used to estimate the errors in Figure 3). The uncertainties on the ratios in the middle and bottom subpanels are the jackknife errors on the ratios themselves, which are significantly smaller than propagating the individual measurement errors, as can be seen by comparing the red and blue shaded regions in the middle subpanels with the gray shaded regions in the middle subpanels (the jackknife measurement errors for the full sample). This is expected as the variations of the different auto-correlation and cross-correlation functions among the different jackknife samples are naturally correlated. (Note that the y-axis range in the two subpanels is different and the gray uncertainty regions plotted in the top and bottom parts of the figure are identical.)

We start by examining the top subpanel in the left side of Figure 10, which illustrates the dependence of clustering on environment. We find distinct differences on large scales between the clustering of the galaxies in the densest environments versus the least dense regions. The galaxies in dense environments are significantly more clustered than the full sample, while the galaxies in the underdense regions are much less clustered, as expected. The cross-correlation functions do not have the same shape on large scales as the full auto-correlation function, due to the way these samples were defined using the $5h^{-1}$ Mpc Gaussian-smoothed density fields, which effectively carves out different regions of dense and underdense environments as seen in Figure 1. In particular, the cross-correlation function for the underdense regions exhibits a fairly sharp dropoff above $\sim 1h^{-1}$ Mpc and goes below 0 at $\gtrsim 3h^{-1}$ Mpc (which is where we stop plotting $\log \xi$).

The middle subpanel shows the ratios of the cross-correlations of the subsamples to the full sample auto-correlation and highlights the dependence on environment. These differences arise due to the dependence of clustering on large-scale environment, i.e, halos in dense environments are more clustered than halos of the same mass in underdense environments. We stress that this dependence by itself is *not* what is commonly referred to as galaxy assembly bias. To illustrate this, we also plot the correlation functions of the shuffled galaxies, where galaxies are randomly assigned to halos of the same mass, which eliminates any connection to the assembly history of the halos. These correlation functions (the dashed lines) show essentially the same trends with environment. This is in agreement with the conclusions of Abbas & Sheth (2005, 2006), who demonstrate that the clustering dependence on large-scale environment can for the most part be

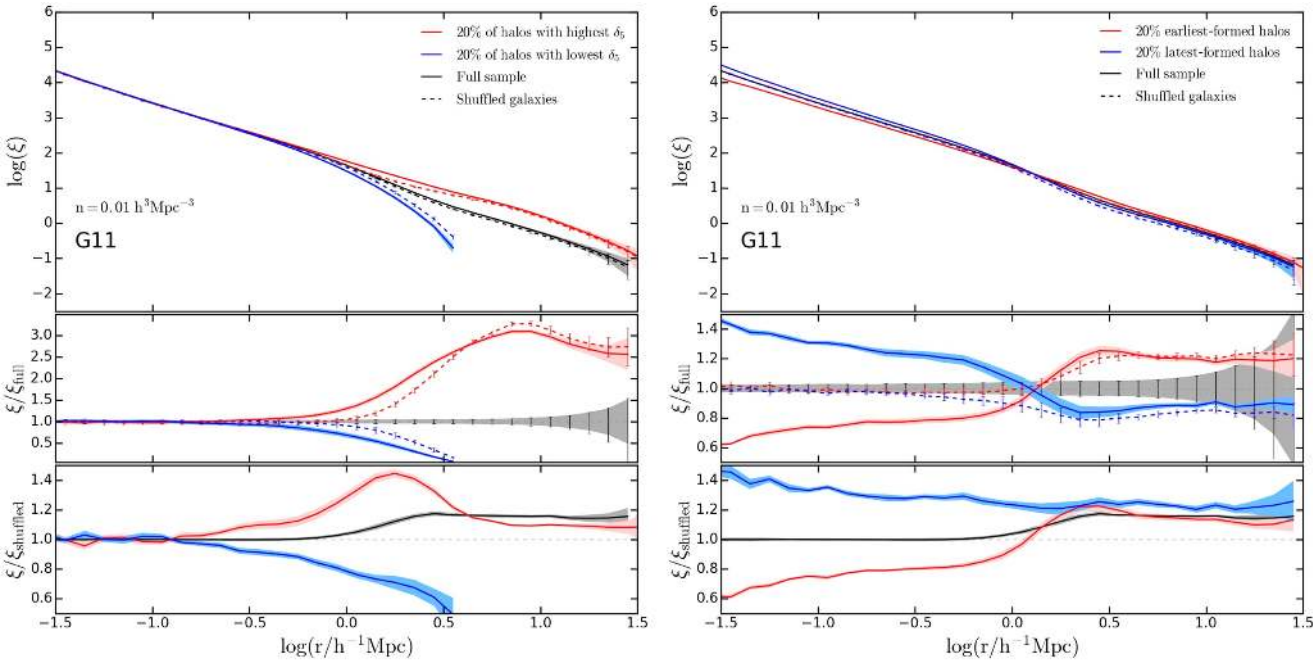

Figure 10. Correlation functions for the G11 $n = 10^{-2}\,h^3$ Mpc^{-3} sample. Left panel: the top subpanel shows the auto-correlation function of the full galaxy sample (black solid line) and the cross-correlation functions of the full sample and galaxies in the 20% of halos in the most and least dense regions (solid red and blue lines, respectively). Dashed lines are the corresponding correlation functions of the shuffled galaxies (see the text). The middle subpanel displays these now divided by the full sample auto-correlation function, highlighting the different clustering properties in different environments. This is shown for both original and shuffled galaxy samples, e.g., the dashed red line is the ratio of the cross-correlation of the shuffled galaxies in the dense regions and the auto-correlation of the full shuffled sample. The bottom subpanel shows, for the three cases, the ratio between the correlation functions of the original and shuffled galaxy samples. In all subpanels, the shaded regions represent the error bars estimated from 10 jackknife realizations. Right panel: same as in the left panel, but now for galaxies residing in halo samples chosen by their formation redshift instead of environment. Red (blue) lines correspond to the cross-correlation function of the full galaxy sample with the subset of galaxies residing in the 20% earliest- (latest-)formed halos.

explained without resorting to occupancy variation (see also Abbas & Sheth 2007; Shi & Sheth 2018).

The differences between the solid and dashed lines (in the top and middle subpanels of Figure 10) reflect the galaxy assembly bias. Namely, the occupancy variation we quantified in the HOD coupled with the environment-dependent halo clustering gives rise to these systematic differences in the galaxy clustering. We illustrate these in detail in the bottom subpanel, which plots the ratio of the original to shuffled correlation functions. We find that the HOD differences with environment do induce significant differences in the large-scale clustering, where for the full sample the clustering of galaxies is stronger by about 15% than the clustering of the shuffled galaxies (with no occupancy variation and thus no galaxy assembly bias). This translates to a ∼7% change in the galaxy bias, in good agreement with the predictions of Croton et al. (2007). The subsample of galaxies in the densest environments exhibits a similar trend, while the galaxies in the least dense regions are significantly less clustered than their shuffled counterparts over most of the range shown. We discuss in Section 5.3 possible reasons for this difference.

The right side of Figure 10 investigates the dependence of clustering on halo age. We see that galaxies in the earliest-formed halos are more clustered on large scales than galaxies in the latest-forming halos. The clustering differences in this case are much smaller than the differences with large-scale environment and have similar shapes. This can be readily seen in the top and middle subpanels, and we remind the reader that the *y*-axis in the middle subpanel for halo age spans a much smaller range than the corresponding one for environment. Again, we note that while these differences are directly due to age-dependent halo clustering, namely reflecting halo assembly bias, these trends only marginally depend on the occupancy variation with age, as seen by the relatively small differences on large scales between the solid and dashed lines in the middle subpanel.

The small-scale clustering in this case shows bigger differences between the solid and dashed lines (that are noticeable in all subpanels). This arises mostly because of the large differences in the satellite occupation functions, as seen in right panel of Figure 3. There are relatively more satellites in late-formed halos versus early-formed halos, especially at the lower-mass end of halos that host satellites, likely simply due to having more time for the satellites to be destroyed in the early-forming halos. This leads to a reversal of the clustering trend (most notable in the middle panel at $r \sim 1\ h^{-1}$ Mpc) and a stronger small-scale clustering for the galaxies in the most recently forming halos. Interestingly, this is then a case where there is no halo assembly bias but galaxy clustering is still different due to occupancy variation with halo age. This feature is evident only for the clustering as a function of halo age and is negligible for the dependence on environment, since in the latter case the differences between the satellite occupations are minuscule (as we have seen in the left panel of of Figure 3).

The bottom subpanel focuses on the galaxy clustering differences due to the occupancy variations by showing the ratio of the correlation functions of the original galaxy samples to the shuffled ones. On small scales, we can see the strong signature of the satellite occupancy variation that we had just discussed (differences between the blue and red lines in the one-halo regime below $r \sim 1\ h^{-1}$ Mpc). The ratio for the full sample (black line) on these scales remains unity, since the

shuffling does not alter at all the one-halo contribution in that case. On larger scales, in the two-halo regime, we see that all three samples exhibit a similar galaxy assembly bias trend, where the clustering of galaxies is stronger than that of the shuffled galaxies. We discuss this further below.

5.3. Origin of Galaxy Assembly Bias Trends

We note an additional subtle feature in the middle subpanel in the right part of Figure 10. As we explained above, the large-scale clustering of galaxies as a function of halo age is dominated by the fact that, at fixed mass, early-formed halos cluster more strongly than late-forming halos (i.e., halo assembly bias). This is reflected by the difference between the dashed red and blue lines. When including the occupancy variation (red and blue solid lines), we see that it acts to slightly decrease the clustering differences between early- and late-formed halos, for separations larger than $\sim 5\ h^{-1}$ Mpc.

These small differences can be understood by examining the changes to the HOD (as shown in the right panel of Figure 3). The central galaxy occupation function for the late-forming halos is shifted toward higher halo masses, which acts to slightly increase their clustering (the blue solid line being above the blue dashed line in the middle subpanel corresponding to formation time). Conversely, the central galaxy occupation function for the early-formed halos is shifted toward lower halo masses, resulting in a slightly reduced clustering (the red solid line lying slightly below the red dashed line). The interpretation gets a bit more complicated since an opposite trend is seen for the satellites; however, we have calculated the effective bias corresponding to these varying HODs and confirmed that the net effect is as described above. We further corroborate this origin of the trend by examining the clustering of the different samples when considering only the central galaxies while excluding the satellites.

We now turn back to the galaxy assembly bias trends shown in the bottom subpanels in Figure 10, for both halo age and environment, where we plotted the clustering of the different samples compared to the clustering of shuffled galaxies where the occupancy variation was erased. When comparing the galaxy assembly trends for halo age and environment, we find a similar effect for the galaxies in early-formed halos and for the galaxies in dense environments (the red solid lines in the two bottom subpanels). The clustering difference is in the same sense for galaxies in late-forming halos (blue solid line in the bottom subpanel of the bottom part of the figure). However, for galaxies in the least dense environments, this trend reverses, with a weaker clustering than that of the shuffled sample (blue solid line in the bottom subpanel of the top part of the figure). We attempt to obtain some insight here regarding the origin of these trends.

We first consider the trends with regard to halo age. In that case, we see that regardless of the sample used (full sample, early forming, or late forming), the galaxy assembly bias trends go in the same direction, with the clustering of galaxies stronger than that of the shuffled samples. We can understand why that is by examining the variations in the central galaxy HOD in Figure 3 and the systematic dependence on halo age in the central galaxies SMHM relation (Figure 9). For any halo mass, we see that central galaxies tend to occupy first the earlier-formed halos. Thus, it is always the case—for any range of halo ages—that the relatively earlier-formed halos will be preferentially populated. Coupling this with the halo assembly bias, namely the stronger clustering of early-formed halos (for a fixed halo mass), results in these galaxies being more clustered than one would expect otherwise. Therefore, the clustering of *any* such sample would always be stronger than the clustering of the corresponding shuffled sample.

The variations in the magnitude of the effect can be explained by looking at the role of the occupancy variation for the satellite galaxies. For the galaxies in the 20% latest-formed halos (the blue solid line), this effect is in fact even more prominent. It arises because these halos also have relatively more satellites (compared to the same halos in the shuffled case), which acts to increase the clustering further (via central–satellite galaxy pairs that contribute as well to the large-scale clustering). On the other hand, the 20% earliest-forming halos have relatively fewer satellites (compared to the same halos in the shuffled case or relative to the HOD for the full sample), and this acts to decrease the clustering and slightly reduce the amplitude of the effect.

For the large-scale environment, we similarly find preferential formation of central galaxies in dense environments. This again implies that halos in relatively denser environments tend to be more populated, and as these halos are more strongly clustered, the galaxies in such halos end up being more clustered (compared to the shuffled galaxies). However, the central galaxy occupancy variation is more nuanced for the environment than for the halo age and the satellites trend is different for them, so the interpretation is more complex. In particular, it is non-trivial to explain the sense of the galaxy assembly bias for the underdense regions, where the clustering is weaker than for the corresponding shuffled sample. From its occupancy variation, it appears that there are fewer satellites overall in that case (for all halo masses), which is possibly the origin of the reduced clustering we measure.

To confirm this explanation, we calculate the effective bias for the different HOD variants by integrating over the halo mass function weighted by the different occupation functions. For the HOD of the underdense regions, we find a reduced effective bias compared to that of the full (or shuffled) sample. When calculating this separately for the central and satellite galaxy occupations, we find that the central galaxy term increases a little while the satellite galaxy term decreases, in agreement with the overall effect, leading to the reduced clustering.

We have also examined the clustering results for the L12 model, for which there is no change in the satellite galaxy occupation function with environment (Figure 4), to aid our understanding of the role the satellites play here. The magnitude of the galaxy assembly bias for the underdense regions in that case is significantly smaller (but still in the same sense as for G11). For lower number density samples (corresponding to more massive galaxies), we find that the galaxy assembly bias even switches sign, i.e., the L12 cross-correlation function for the underdense regions is more strongly clustered than the shuffled case (while the trend remains unchanged for G11). This further indicates that the trend observed for G11 for the underdense regions is due to the satellite occupancy variation.

Finally, we also measured the clustering of the G11 subsamples, when considering only central galaxies. We find similar galaxy assembly bias trends for the full sample and the dense regions, and a much reduced effect for the underdense regions. This again supports our understanding that the satellite galaxy occupancy variation is the main cause of the unique

galaxy assembly bias we see for the underdense regions, while the central occupancy variation is the dominant factor in all other cases. This difference may also be related to the general shape of the cross-correlation function for the underdense regions (induced by the large smoothing window) and the relative bias factor becoming negative on large scales (when the cross-correlation function goes below zero).

6. Summary and Conclusion

We have utilized semi-analytic models applied to the Millennium simulation to study the occupancy variation leading to galaxy assembly bias. We studied in detail the explicit dependence of the halo occupation functions on large-scale environment, defined as the $5\,h^{-1}$ Mpc Gaussian-smoothed dark matter density field, and on halo formation time, defined as the redshift at which the halo gained (for the first time) half of its present-day mass. Although related, these two halo properties have only a very loose relation between them and probe different distributions of halos. We focus our analysis on the 20% subsets of halos at the extremes of the distributions of each property, defined separately for each halo mass bin, so as to eliminate the dependence of the halo mass function on these properties. We then study the different occupation functions of the galaxies in these halos and investigate the origin of the variations. We stress that in all analyses done here, the HODs are calculated directly from the SAM galaxy catalogs, and not inferred from clustering measurements. Our key results are shown in Figures 3, 9, and 10.

For the dependence on environment, we find small but distinct differences in the HOD, especially at the "knee" of the central occupation function. The central galaxies in dense environments start populating lower-mass halos, and conversely, central galaxies in underdense environments are more likely to be hosted by more massive halos. This trend is robust among the two SAMs we studied. For one of the SAMs (G11), the satellite occupation function shows similar trends to the centrals, while the other (L12) does not exhibit variation for the satellites. We quantify the occupancy variations in terms of the changes to the HOD parameters.

When studying the dependence on halo formation redshift (halo age), we find similar but significantly stronger trends for the central occupation functions. The satellite occupation function shows the reverse trend, where the early-formed halos tend to have much fewer satellites than late-formed halos. This likely arises from having more time for the satellites to merge with the central galaxy in the older halos. The relatively stronger trends for halo age suggest that this is the more fundamental property (among the two) giving rise to galaxy assembly bias.

We gain insight into the origin of the central galaxy occupancy variation by examining the scatter in the SMHM relation for them and its correlation with halo age and environment. We find that, at fixed halo mass, central galaxies in early-formed halos or dense environments tend to be more massive. This directly leads to the occupancy variation we observe, as for any stellar-mass-limited sample, the more massive central galaxies will be "picked" first in lower-mass halos. The dependence on halo age is very distinct, while the dependence on environment shows more scatter, resulting in weaker trends with environment. The dependence of the centrals stellar mass on halo age can be easily explained as the central galaxies in the early-formed halos have more time to accrete and form more stars. These correlations, and the resulting occupancy variation, thus depend on the specific details of the galaxy formation model. This direct link to the correlated nature of the stellar mass–halo mass relation also has important implications for models that use subhalo abundance matching to connect galaxies with their host halos.

We also examine the auto-correlation and cross-correlation functions of these different samples, and the impact of these occupancy variations, by comparing to the clustering of shuffled galaxy samples where the occupancy variation has been erased. We demonstrate the stronger clustering signal of galaxies in the densest regions versus the least dense regions, and similarly the strong clustering of galaxies in early-formed halos versus late-formed ones. We clarify that while these clustering differences arise from the dependence of halo clustering on halo age and environment, they are only marginally affected by the occupancy variations (and are not what we refer to as galaxy assembly bias).

For all samples defined by halo age, the clustering of galaxies is stronger than that of the shuffled samples. Namely, we see that the occupation variation coupled with the halo assembly bias acts to increase the clustering of galaxies. This effect is explained and dominated by the central galaxy occupancy variation. For any range of halo ages, the earlier-formed halos are preferentially populated. Since these halos are more strongly clustered, the net effect is a stronger clustering of the galaxies. The satellite occupancy variation further modulates this effect, but it is secondary here. The same behavior is found for the full sample of galaxies and for galaxies in dense environments. This again is due to the tendency to preferentially populate the halos in denser environments, which are in turn more strongly clustered. The galaxies in the most underdense regions exhibit the opposite trend, however, with weaker clustering than in the corresponding shuffled sample. This behavior is less intuitive, but is likely caused by the satellite galaxy occupancy variation, as discussed.

Our approach here has already provided considerable insight into the nature and origin of this complex phenomena. A companion paper (S. Contreras et al. 2018, in preparation) is studying the redshift dependence of the occupancy variation and galaxy assembly bias in the SAMs, which provides a comprehensive view of the evolution of the different trends. We are also investigating the occupancy variation with age and environment in the EAGLE and Illustris cosmological hydrodynamical simulations (M. C. Artale et al. 2018, in preparation).

Our study can inform theoretical models of assembly bias as well as attempts to determine it with observational data. Additionally, it can facilitate creating mock catalogs that incorporate this effect, to aid in preparation for future surveys and in evaluating the impact of galaxy assembly bias on cosmological analyses. What the level of assembly bias is in the real universe remains an open (and hotly debated) question. We are hopeful that this work can set the stage to developing and applying a method that will conclusively determine that.

This work was made possible by the efforts of Gerard Lemson and colleagues at the German Astronomical Virtual Observatory in setting up the Millennium Simulation database in Garching, and John Helly and Lydia Heck in setting up the mirror at Durham. We thank Celeste Artale, Shaun Cole, Ravi Sheth, and Zheng Zheng for useful discussions, and Ivan

Lacerna, Gary Mamon, and the anonymous referee for helpful comments. I.Z., S.C., and N.P. acknowledge the hospitality of the ICC at Durham and the helpful conversations with many of its members. I.Z. and P.N. also acknowledge the participants of the KITP Galaxy–Halo Connection workshop for stimulating discussions in the final stages of this work. I.Z. and N.J.S. acknowledge support by NSF grant AST-1612085. I.Z. was further supported by a CWRU Faculty Seed Grant. P.N. and I.Z. acknowledge support from the European Research Council, through the ERC Starting Grant DEGAS-259586. We acknowledge support from the European Commissions Framework Programme 7, through the Marie Curie International Research Staff Exchange Scheme LACEGAL (PIRSES-GA-2010-269264) and from an STFC/Newton Fund award (ST/M007995/1-DPI20140114). S.C. further acknowledges support from the CONICYT Doctoral Fellowship Programme and from the European Research Council through grant No. ERC-StG/716151. N.P. is supported by "Centro de Astronomía y Tecnologías Afines" BASAL PFB-06 and by Fondecyt Regular 1150300. C.M.B. and P.N. additionally acknowledge the support of the Science and Technology Facilities Council (ST/L00075X/1). P.N. further acknowledges the support of the Royal Society through the award of a University Research Fellowship. The calculations for this paper were performed on the ICC Cosmology Machine, which is part of the DiRAC-2 Facility jointly funded by STFC, the Large Facilities Capital Fund of BIS, and Durham University and on the Geryon computer at the Center for Astro-Engineering UC, part of the BASAL PFB-06, which received additional funding from QUIMAL 130008 and Fondequip AIC-57 for upgrades.

Appendix A
Sample Cuts

As described in Section 3.1, we define our density and halo age samples by ranking the halos according to the property at hand in narrow bins of halo mass and then selecting the two 20% extremes in each bin. Our cuts therefore directly depend on halo mass. The motivation for this procedure is to remove the dependence of the halo mass function on these properties, effectively ensuring that (for either halo age or environment) the two 20% samples have the same halo mass functions. This allows for a cleaner comparison of the different HODs, using halos of nearly equal mass for the two extremes.

Figure 11 shows how our environment and halo age sample cuts vary with halo mass. The left panel in Figure 11 shows the environmental dependence of halo mass, reflecting the known fact that massive halos tend to reside in dense environments. The middle solid line is the median value as a function of halo mass and the shaded region is the 20%–80% range of the distribution. This demonstrates the behavior of our halo-mass-dependent density cut, which adjusts for that exhibiting an upturn toward denser environments with increasing halo mass. The curves that bound the shaded regions are exactly the dividing lines defining our different environments, i.e., halos that lie above the top curve belong to the densest 20% and the halos below the bottom curve make up the least dense 20%. The right panel demonstrates how the formation redshift correlates with halo mass, exhibiting the known trend that more massive halos tend to form later. This, again, is explicitly adjusted for by varying the formation redshift boundaries as a function of halo mass, as illustrated.

We note that, in practice, the occupancy variation trends are in fact very similar whether one follows this procedure or not. We have verified this by defining the 20% extremes samples by a global cut in density, independent of halo mass (corresponding to horizontal lines in Figure 11) and repeating our analysis. The clustering of the samples are different in this case, since, for example, the most massive halos would predominantly be included in our densest environment sample and not be represented in the underdense sample. This, however, has little impact on the occupancy variation, which probes the dependence of the HOD on secondary properties

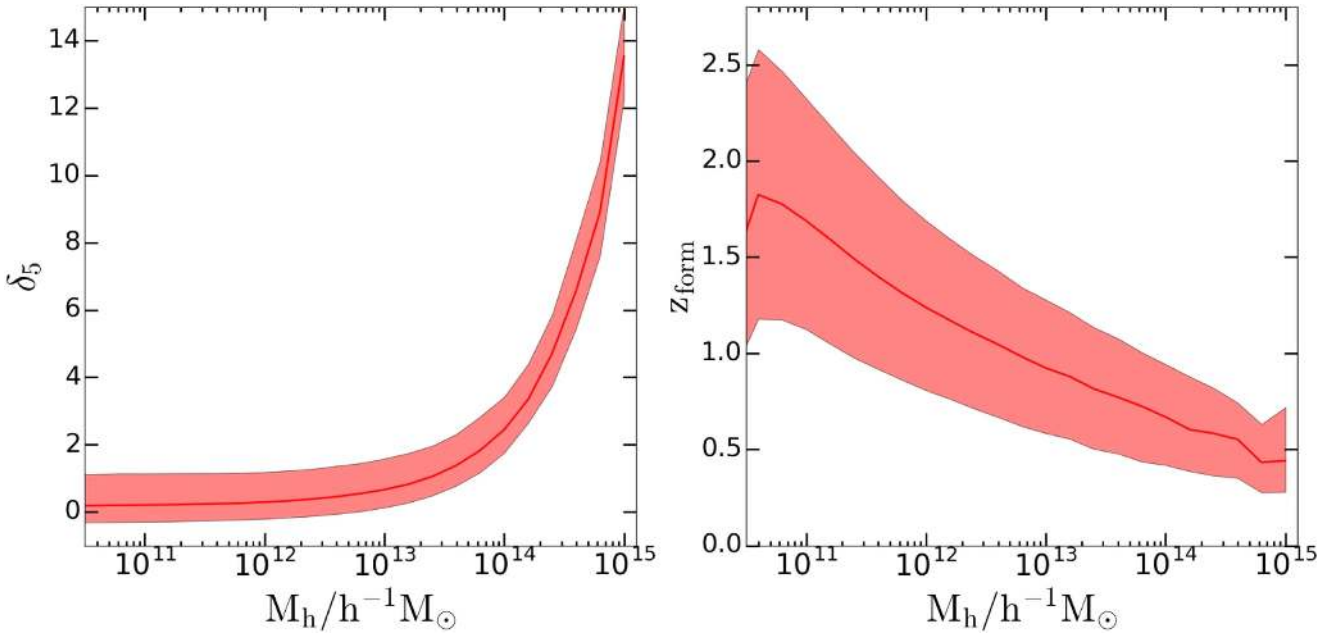

Figure 11. Halo-mass-dependent cuts used to define our samples. The left panel shows how our environment measure δ_5 varies with halo mass. The solid line is the median value of the density for each halo mass bin, and the shaded region represents the 20%–80% range of its distribution. The right panel shows the same but now for halo age as a function of halo mass.

other than halo mass. The main difference in the HODs is that they cannot all be calculated over the same halo mass range in that case.

Appendix B
Auto-correlation Functions

In Section 5.2, we analyze in detail the clustering results of the different samples, using the cross-correlation functions between the full galaxy sample and the different subsamples. Here we present the corresponding results for the auto-correlation functions and explain our motivation for preferring one over the other.

Figure 12 illustrates these results for the galaxy samples selected according to halo age. We find a distinct difference in the shape of the auto-correlation functions for galaxies in the early- and late-forming halos (red and blue solid lines, respectively, in the top panel), where both exhibit a stronger clustering signal than the auto-correlation of the full sample (black solid line) on scales smaller than $\sim 1\ h^{-1}$ Mpc. This excess clustering gradually diminishes for scales larger than that, over roughly the 1–7 h^{-1} Mpc range. Although perhaps surprising at first glance, this feature arises due to the way the samples are created. In all such subsamples, 20% of the halos are chosen according to a specific halo property, and then all galaxies in these halos are included in the sample. This is systematically a very different selection than if we chose ∼20% of the galaxies without enforcing the inclusion of all galaxies in a given halo. It acts to "artificially" increase the small-scale clustering of galaxies mostly due to the contribution of satellite–satellite pairs to the one-halo term in the galaxy auto-correlation function. This excess clustering naturally decreases when going to scales larger than the size of the halos.

To confirm this explanation, we study another galaxy subsample in which we choose 20% of the halos completely at random and then compute the auto-correlation function of all galaxies belonging to these randomly chosen halos (shown as the solid gray line in the top panel). We see that this sample also exhibits this excess clustering on small scales, lying in between the auto-correlation functions of the two other subsamples and then converges with the auto-correlation function of the full sample on large scales. We also performed the simple test of choosing 20% of the galaxies completely at random, irrespective of which halos they belong to. In that case (not included in Figure 12), we get the expected result that this random subset has an identical clustering to the full sample.

This behavior of the auto-correlation functions, while completely understood, is the main reason we prefer to showcase the cross-correlation results in the main part of the paper. The auto-correlation functions for the samples defined by the environment (not shown here) exhibit the same behavior. Other than this feature, the rest of the trends are similar whether one studies them with the auto-correlation functions or the cross-correlation functions, as can be seen in the middle and bottom panels. One just has to be careful to account for the different bias factors that come into the ratios in each case. The auto-correlation function measurements are also slightly noisier, which is also reflected in the larger error bars, due to the fact that the number of pairs in this case is smaller by about a factor of 5. This is the other reason we chose to focus on the cross-correlation results.

In the middle panel of Figure 12, we examine the ratio between the clustering of galaxies in the 20% of early- and late-forming halos and that of the galaxies in the random 20% of halos (to eliminate the impact of the small-scale feature). We plot the square root of this ratio since two factors of the relative bias parameter come in the auto-correlation functions ratio, while only one factor is included in the ratio of the cross-correlation function and the full sample auto-correlation function. It is reassuring to see that the trends on large scales are very similar qualitatively and quantitatively. The trends on small scales are also very similar, just with a slight difference in amplitude, likely due to dividing by a larger clustering amplitude.

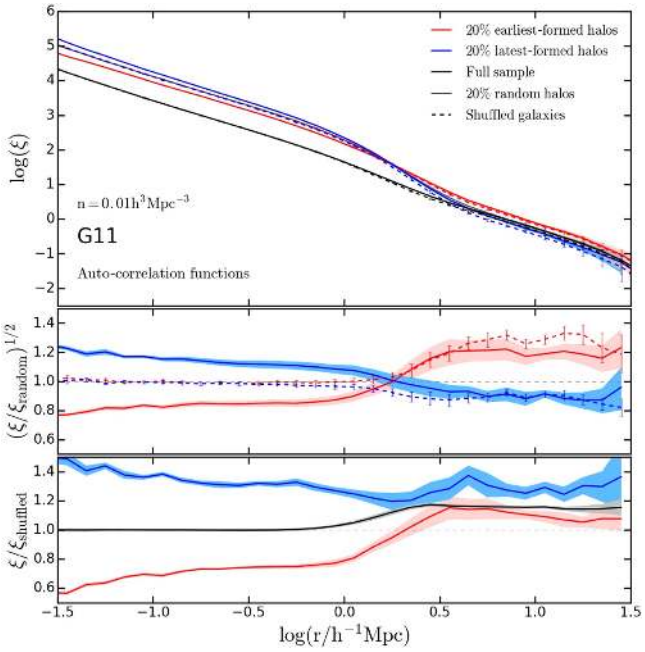

Figure 12. Auto-correlation functions for the G11 $n = 10^{-2}\ h^3$ Mpc^{-3} sample, for galaxies selected by halo age. This plot is analogous to the right side of Figure 10, but now plotting auto-correlation functions for all samples, instead of the cross-correlation functions of the full sample with the galaxies in early-/late-forming halos. Dashed lines are the corresponding correlation functions of the shuffled galaxies, as before. In the top panel, we also add the auto-correlation function of galaxies in a random 20% subset of the halos (gray solid line; see the text). The middle panel shows the correlation functions divided out by the auto-correlation function of this random-halos sample. For consistency with the inferred galaxy bias factors, we plot here the square root of this ratio. The bottom panel shows the ratio between the correlation functions of the original and shuffled samples, for the three main cases. The shaded regions represent the uncertainties estimated from 10 jackknife realizations.

The results for the galaxy assembly bias shown in the bottom panel of Figure 12 are also very similar to the ones obtained from the cross-correlation functions in Figure 10. When comparing the values in detail, one needs to account for the specific "assembly bias factors" (defined in an analogous manner to galaxy bias factors) in each case. For example, for the galaxies in late-forming halos, in the auto-correlation functions ratio, the assembly bias factor for that sample appears twice. In contrast, in the cross-correlation functions ratio, this assembly bias appears only once but gets multiplied by the assembly bias factor for the full galaxy sample. Once that is properly accounted for, the impact of galaxy assembly bias on these two different clustering measures is in excellent agreement.

ORCID iDs

Idit Zehavi https://orcid.org/0000-0001-8286-6024
Sergio Contreras https://orcid.org/0000-0001-7511-7025
Nelson Padilla https://orcid.org/0000-0001-9850-9419

Nicholas J. Smith https://orcid.org/0000-0002-3222-2949
Carlton M. Baugh https://orcid.org/0000-0002-9935-9755
Peder Norberg https://orcid.org/0000-0002-5875-0440

References

Abbas, U., & Sheth, R. K. 2005, MNRAS, 364, 1327
Abbas, U., & Sheth, R. K. 2006, MNRAS, 372, 1749
Abbas, U., & Sheth, R. K. 2007, MNRAS, 378, 641
Angulo, R., Baugh, C. M., & Lacey, C. G. 2008, MNRAS, 387, 921
Artale, M. C., Pedrosa, S. E., Trayford, J. W., et al. 2017, MNRAS, 470, 1771
Baldry, I. K., Glazebrook, K., Brinkmann, J., et al. 2004, ApJ, 600, 681
Balogh, M. L., Baldry, I. K., Nichol, R., et al. 2004, ApJL, 615, L101
Baugh, C. M. 2006, RPPh, 69, 3101
Berlind, A. A., & Weinberg, D. H. 2002, ApJ, 575, 587
Berlind, A. A., Weinberg, D. H., Benson, A. J., et al. 2003, ApJ, 593, 1
Berlind, A. A., Blanton, M. R., Hogg, D. W., et al. 2005, ApJ, 629, 625
Berlind, A. A., Kazin, E., Blanton, M. R., et al. 2006, arXiv:0610524
Blanton, M. R., Eisenstein, D. J., Hogg, D. W., Schlegel, D. J., & Brinkmann, J. 2005, ApJ, 629, 143
Blanton, M. R., Eisenstein, D. J., Hogg, D. W., & Zehavi, I. 2006, ApJ, 645, 977
Blanton, M. R., & Berlind, A. A. 2007, ApJ, 664, 791
Blanton, M. R., & Moustakas, J. 2009, ARA&A, 47, 159
Bond, J. R., Cole, S., Efstathiou, G., & Kaiser, N. 1991, ApJ, 379, 440
Borzyszjowski, M., Porciani, C., Romano-Diaz, E., & Geraldi, E. 2017, MNRAS, 469, 594
Bower, R. G., Benson, A. J., Malbon, R., et al. 2006, MNRAS, 370, 645
Bray, A. D., Pillepich, A., Sales, L. V., et al. 2016, MNRAS, 455, 185
Busch, P., & White, S. D. M. 2017, MNRAS, 470, 4767
Campbell, D., van den Bosch, F. C., Hearin, A., et al. 2015, MNRAS, 452, 444
Chaves-Montero, J., Angulo, R. E., Schaye, J., et al. 2015, MNRAS, 460, 3100
Cole, S., Lacey, C. G., Baugh, C. M., & Frenk, C. S. 2000, MNRAS, 319, 168
Contreras, S., Baugh, C. M., Norberg, P., & Padilla, N. 2014, MNRAS, 432, 2717
Contreras, S., Baugh, C. M., Norberg, P., & Padilla, N. 2015, MNRAS, 452, 1861
Contreras, S., Zehavi, I., Baugh, C. M., Padilla, N., & Norberg, P. 2017, MNRAS, 465, 2833
Cooper, M. C., Gallazzi, A., Newman, J. A., & Yan, R. 2010, MNRAS, 402, 1942
Cooray, A., & Sheth, R. 2002, PhR, 372, 1
Coupon, J., Kilbinger, M., & McCracken, H. J. 2012, A&A, 542, 5
Croft, R. A. C., Matteo, T. D., Khandai, N., et al. 2012, MNRAS, 425, 2766
Croton, D. J., & Farrar, G. R. 2008, MNRAS, 386, 2285
Croton, D. J., Gao, L., & White, S. D. M. 2007, MNRAS, 374, 1303
Croton, D. J., Springel, V., White, S. D. M., et al. 2006, MNRAS, 365, 11
Dalal, N., White, M., Bond, J. R., & Shirokov, A. 2008, ApJ, 687, 12
Davis, M., Efstathiou, G., Frenk, C. S., & White, S. D. M. 1985, ApJ, 292, 371
De Lucia, G., & Blaizot, J. 2007, MNRAS, 375, 2
De Lucia, G., Kauffmann, G., & White, S. D. M. 2004, MNRAS, 349, 1101
Deason, A. J., Conroy, C., Wetzel, A. R., & Tinker, J. L. 2013, ApJ, 777, 154
Desjacques, V. 2008, MNRAS, 388, 638
Dressler, A. 1980, ApJ, 236, 351
Dvornik, A., Cacciato, M., Kuijken, K., et al. 2017, MNRAS, 468, 3251
Font, A. S., Bower, R. G., McCarthy, I. G., et al. 2008, MNRAS, 389, 1619
Gao, L., Springel, V., & White, S. D. M. 2005, MNRAS, 363, L66
Gao, L., & White, S. D. M. 2007, MNRAS, 377, L5
Giocoli, C., Giuseppe, T., Sheth, R. K., & van den Bosch, F. C. 2010, MNRAS, 404, 502
Guo, H., Zheng, Z., Zehavi, I., et al. 2014, MNRAS, 441, 2398
Guo, Q., Gonzalez-Perez, V., Guo, Q., et al. 2016, MNRAS, 461, 3457
Guo, Q., White, S., Boylan-Kolchin, M., et al. 2011, MNRAS, 413, 101 [G11]
Guo, Q., White, S. D. M., Angulo, R. E., et al. 2013, MNRAS, 428, 1351
Hahn, O., Porciani, C., Dekel, A., & Carollo, C. M. 2009, MNRAS, 398, 1742
Harker, G., Cole, S., Helly, J., Frenk, C., & Jenkins, A. 2006, MNRAS, 367, 1039
Hearin, A. P., & Watson, D. F. 2013, MNRAS, 435, 1313
Hearin, A. P., Watson, D. F., & van den Bosch, F. C. 2015, MNRAS, 452, 1958
Hogg, D. W., Blanton, M. R., Eisenstein, D. J., et al. 2003, ApJL, 585, L5
Jiang, L., Helly, J. C., Cole, S., & Frenk, C. S. 2014, MNRAS, 440, 2115
Jiang, F., & van den Bosch, F. C. 2017, MNRAS, 472, 657
Jing, Y. P., Suto, Y., & Mo, H. J. 2007, ApJ, 657, 664
Jung, I., Lee, J., & Yi, S. K. 2014, ApJ, 794, 74
Keselman, J. A., & Nusser, A. 2007, MNRAS, 382, 1853
Kravtsov, A. V., Berlind, A. A., Wechsler, R. H., et al. 2004, ApJ, 609, 35
Lacerna, I., & Padilla, N. 2011, MNRAS, 412, 1283
Lacerna, I., Padilla, N., & Stasyszyn, F. 2014a, MNRAS, 443, 3107
Lacerna, I., Rodriguez-Puebla, A., Avila-Reese, V., & Hernandez-Toledo, H. M. 2014b, ApJ, 788, 29
Lacerna, I., Contreras, S., Gonzalez, R. E., Padilla, N., & Gonzalez-Perez, V. 2017, MNRAS, in press (arXiv:1703.10175)
Lacey, C. G., Baugh, C. M., Frenk, C. S., et al. 2016, MNRAS, 462, 3854
Lagos, C. d. P., Baugh, C. M., Lacey, C. G., et al. 2011, MNRAS, 418, 1649
Lagos, C. d. P., Bayet, E., Baugh, C. M., et al. 2012, MNRAS, 426, 2142
Lazeyras, T., Musso, M., & Schmidt, F. 2017, JCAP, 3, 59
Lemson, G., & Kauffmann, G. 1999, MNRAS, 302, 111
Lewis, I., Balogh, M., De Propris, R., et al. 2002, MNRAS, 334, 673
Lin, Y., Mandelbaum, R., Huang, Y., et al. 2016, ApJ, 819, 119
Ludlow, A. D., & Porciani, C. 2011, MNRAS, 406, 137
Mao, Y., Zentner, A. R., & Wechsler, R. H. 2018, MNRAS, 474, 5143
Matthee, J., Schaye, J., Crain, R., et al. 2017, MNRAS, 465, 2381
McCullagh, N., Norberg, P., Cole, S., et al. 2017, MNRAS, submitted (arXiv:1705.01988)
McEwen, J. E., & Weinberg, D. H. 2016, arXiv:1601.02693
Mehta, K. T. 2014, PhD Thesis, The University of Arizona
Merson, A. I., Baugh, C. M., Helly, J. C., et al. 2013, MNRAS, 429, 556
Mitchell, P. D., Lacey, C. G., Baugh, C. M., & Cole, S. 2016, MNRAS, 456, 1459
Miyatake, H., More, S., Takada, M., et al. 2016, PhRvL, 116, 041301
Mo, H. J., & White, S. D. M. 1996, MNRAS, 282, 347
Montero-Dorta, A. D., Perez, E., Prada, F., et al. 2017, ApJL, 848, L2
Muldrew, S. I., Croton, D. J., Skibba, R. A., et al. 2012, MNRAS, 419, 2670
Oemler, A. 1974, ApJ, 194, 1
Peacock, J. A., & Smith, R. E. 2000, MNRAS, 318, 1144
Pujol, A., & Gaztanaga, E. 2014, MNRAS, 442, 1930
Reed, D., Governato, F., Quinn, T., Stadel, J., & Lake, G. 2007, MNRAS, 378, 777
Romano-Diaz, E., Garaldi, E., Borzyszkowski, M., & Porciani, C. 2017, MNRAS, 469, 1809
Sandvik, H. B., Moller, O., Lee, J., & White, S. D. M. 2007, MNRAS, 377, 234
Saito, S., Leauthaud, A., Hearin, A. P., et al. 2016, MNRAS, 460, 1457
Schaye, J., Crain, R. A., Bower, R. G., et al. 2015, MNRAS, 446, 521
Scoccimarro, R., Sheth, R. K., Hui, L., & Jain, B. 2001, ApJ, 546, 20
Seljak, U. 2000, MNRAS, 318, 203
Seo, H.-J., Eisenstein, D. J., & Zehavi, I. 2008, ApJ, 681, 998
Sheth, R. K., & Tormen, G. 2004, MNRAS, 350, 1385
Shi, J., & Sheth, R. K. 2018, MNRAS, 473, 2486
Sin, L. P. T., Lilly, S. J., & Henriques, B. M. B. 2017, MNRAS, 471, 1192
Skibba, R. A., Sheth, R. K., Connolly, A. J., & Scranton, R. 2006, MNRAS, 369, 68
Skibba, R. A., Coil, A. L., Mendez, A. J., et al. 2015, ApJ, 807, 152
Somerville, R. S., & Davé, R. 2015, ARA&A, 53, 51
Springel, V., White, S. D. M., Jenkins, A., et al. 2005, Natur, 435, 629
Springerl, V., White, S. D. M., Tormen, G., & Kauffmann, G. 2001, MNRAS, 328, 726
Tinker, J. L., Conroy, C., Norberg, P., et al. 2008a, ApJ, 686, 53
Tinker, J. L., Wetzel, A. R., & Conroy, C. 2011, arXiv:1107.5046
Tinker, J. L., George, M. R., Leauthaud, A., et al. 2008b, ApJL, 755, L5
Tinker, J. L., Hahn, C., Mao, Y., Wetzel, A. R., & Conroy, C. 2017a, MNRAS, submitted (arXiv:1702.01121)
Tinker, J. L., Hahn, C., Mao, Y., & Wetzel, A. R. 2017b, MNRAS, submitted (arXiv:1705.08458)
Tojeiro, R., Eardley, E., Peacock, J. A., et al. 2017, MNRAS, 470, 3720
Tonnesen, S., & Cen, R. 2015, ApJ, 812, 104
Vakili, M., & Hahn, C. H. 2016, ApJ, submitted (arXiv:1610.01991)
van den Bosch, F. C., Tormen, G., & Carlo, G. 2005, MNRAS, 359, 1029
Vogelsberger, M., Genel, S., Springel, V., et al. 2014, MNRAS, 444, 1518
Wang, Y., Yang, X., Mo, H. J., et al. 2008, ApJ, 687, 919
Wang, L., Weinmann, S. M., & De Lucia, G. 2013a, MNRAS, 431, 600
Wang, L., Weinmann, S. M., De Lucia, G., & Yang, X. 2013b, MNRAS, 433, 515
Watson, D. F., Berlind, A. A., & Zentner, A. R. 2011, ApJ, 738, 22
Watson, D. F., Hearin, A. P., Berlind, A. A., et al. 2015, MNRAS, 446, 651
Wechsler, R. H., Zentner, A. R., Bullock, J. S., Kravtsov, A. V., & Allgood, B. 2006, ApJ, 652, 71
Wetzel, A. R., Cohn, J. D., White, M., Holz, D. E., & Warren, M. S. 2007, ApJ, 656, 139

White, S. 1999, Ap&SS, 267, 355
Xu, X., & Zheng, Z. 2017, MNRAS, submitted (arXiv:1710.06862)
Yang, X. H., Mo, H. J., & van den Bosch, F. C. 2006, ApJL, 638, L55
Zehavi, I., Weinberg, D. H., Zheng, Z., et al. 2004, ApJ, 608, 16
Zehavi, I., Zheng, Z., Weinberg, D. H., et al. 2005, ApJ, 630, 1
Zehavi, I., Zheng, Z., Weinberg, D. H., et al. 2011, ApJ, 736, 59
Zentner, A. R., Berlind, A. A., Bullock, J. S., Kravtsov, A. V., & Wechsler, R. H. 2005, ApJ, 624, 505
Zentner, A. R. 2007, IJMPD, 16, 763
Zentner, A. R., Hearin, A. P., & van den Bosch, F. C. 2014, MNRAS, 443, 3044
Zentner, A. R., Hearin, A., van den Bosch, F. C., Lange, J. U., & Villarreal, A. 2016, MNRAS, submitted (arXiv:1606.07817)
Zhang, J., Ma, C., & Riotto, A. 2014, ApJ, 782, 44
Zheng, Z., Berlind, A. A., Weinberg, D. H., et al. 2005, ApJ, 633, 791
Zheng, Z., Coil, A. L., & Zehavi, I. 2007, ApJ, 667, 760
Zhu, G., Zheng, Z., Lin, W. P., et al. 2006, ApJL, 639, L5
Zu, Y., & Mandelbaum, R. 2016, MNRAS, 457, 4360
Zu, Y., & Mandelbaum, R. 2017, arXiv:1703.09219
Zu, Y., Mandelbaum, R., Simet, M., Rozo, E., & Rykoff, E. S. 2016, MNRAS, 470, 551
Zu, Y., Zheng, Z., Zhu, G., & Jing, Y. P. 2008, ApJ, 686, 41